

## Experimental Investigation Replicating the Surface Behavior of Ground Steel Gears in Mixed Lubrication Using Twin-Disk Testing Part 1: Running-In

W. M. Britton, A. Clarke & H. P. Evans

To cite this article: W. M. Britton, A. Clarke & H. P. Evans (2025) Experimental Investigation Replicating the Surface Behavior of Ground Steel Gears in Mixed Lubrication Using Twin-Disk Testing Part 1: Running-In, Tribology Transactions, 68:1, 121-141, DOI: [10.1080/10402004.2024.2387779](https://doi.org/10.1080/10402004.2024.2387779)

To link to this article: <https://doi.org/10.1080/10402004.2024.2387779>



© 2025 The Author(s). Published with license by Taylor & Francis Group, LLC



Published online: 08 Jan 2025.



Submit your article to this journal [↗](#)



Article views: 258



View related articles [↗](#)



View Crossmark data [↗](#)

# Experimental Investigation Replicating the Surface Behavior of Ground Steel Gears in Mixed Lubrication Using Twin-Disk Testing Part 1: Running-In

W. M. Britton<sup>a,b</sup>, A. Clarke<sup>b</sup>, and H. P. Evans<sup>b</sup>

<sup>a</sup>BMT Limited, Bath, UK; <sup>b</sup>School of Engineering, Cardiff University, Cardiff, UK

## ABSTRACT

The surface of ground gear teeth is changed during the initial period of operation through a process termed running-in. During this process, asperity peaks are plastically deformed and removed to better distribute the load across the surface, resulting in modification of the surface finish. In this work the influence of pressure, slide-roll ratio, and entrainment velocity on two-dimensional surface roughness parameters is evaluated through the running-in process using a full-factorial experimental program. Hardened steel disks are used to simulate gear tooth contacts via the use of a twin-disk rig. Results showed that all three variables strongly influence the change in surface geometry, both individually and through both two- and three-factor interactions.

## ARTICLE HISTORY

Received 1 December 2023  
Accepted 29 July 2024

## KEYWORDS

Mixed lubrication; running-in; gears; elasto-hydrodynamics

## Introduction

Hardened steel gears operating in elasto-hydrodynamic lubrication (EHL) regimes are a fundamental part of many of drivetrain systems in automotive, aircraft, marine, and power generation sectors. The ability to generate a more accurate tooth profile (allowing higher loads to be carried) and produce a consistent surface finish across the entire gear has made ground gears the principal choice for high-load applications. In some safety-critical or high-performance applications, superfinishing is able to improve both life and performance; (1) however, this additional stage of manufacture is not always feasible on grounds of cost and/or gear size (e.g., marine or wind turbine applications).

An engineering trend of operating with lower viscosity lubricants in the name of improved efficiency means that many of these ground gear systems operate in the regime of “Mixed Lubrication,” where the load is carried in part by the EHL film, and in part by direct contact between roughness asperity peaks on the surfaces. Typically, the state of mixed lubrication is defined using the specific film thickness parameter  $\Lambda$  (2) calculated as in Eq. [1], where a value  $0 < \Lambda < 2$  indicates a state of mixed lubrication. (3,4)

$$\Lambda = \frac{h}{\sqrt{R_{q1}^2 + R_{q2}^2}} \quad [1]$$

In this state significant direct contact occurs between asperity peaks on opposing surfaces, inducing plastic deformation and wear which modifies the surface geometry to better distribute the load.

The topic of surface changes through running-in has been explored to a limited extent in the literature. It is known that surface asperities are the features primarily affected by running-in, while valley features remain essentially unchanged during the initial period of contact. (5–7) As such, it has been suggested that changes in the value of the peak height parameter  $R_p$  better reflects the running-in process than the more commonly used  $R_a$  or  $R_q$  parameters. (6) Radii of curvature of asperity tips (8) and wavelength of roughness (via changes in radius of curvature and amalgamation of double-peak features) (9) have also been found to change through running-in.

Lohner et al. (10) investigated the change in  $R_a$ ,  $R_{pk}$ , and  $R_{sk}$  through running-in via both twin-disk experiments and FZG gear tests. These tests found that where  $R_a$  was initially greater, the  $R_a$  tended to retain a higher value at the conclusion of running-in, which is a similar observation to that of Wang et al. (11) Additionally, Lohner observed a greater change in all three of the considered roughness parameters in twin-disk tests when compared to gear tests. This was attributed to the disk surface experiencing a constant boundary friction power, while the gear surface friction was transient.

Sjöberg et al. (12) found that increased load during running-in led to greater surface modification during the running-in process, and also led to improved gear efficiency.

While running-in has most commonly been assessed in terms of the change in two-dimensional profiles, some works have attempted to characterize the running-in process using areal parameters. Prajapati and Tiwari (13) found that  $S_a$ ,  $S_q$ , and  $S_z$  changed through the running-in process, but saw more significant change in less commonly encountered parameters such as autocorrelation length and RMS slope. Likewise,

CONTACT A. Clarke  [Clarkea7@cardiff.ac.uk](mailto:Clarkea7@cardiff.ac.uk)  
Review led by S. Berkebile.

© 2025 The Author(s). Published with license by Taylor & Francis Group, LLC

This is an Open Access article distributed under the terms of the Creative Commons Attribution License (<http://creativecommons.org/licenses/by/4.0/>), which permits unrestricted use, distribution, and reproduction in any medium, provided the original work is properly cited. The terms on which this article has been published allow the posting of the Accepted Manuscript in a repository by the author(s) or with their consent.

Cabanettes and Rosen (14) found the more obscure parameters of mean summit curvature, developed interfacial area ratio, and mean slope, to be the primary indicators of change through areal measurements. Martins et al. (15) found maximum roughness parameters showed the clearest change through running-in, while average roughness parameters such as Ra showed less significant change.

Other works, rather than focusing on the changes in surface parameters, have instead investigated the period over which running-in takes place. Through analysis of acoustic emission signals, Hutt et al. (16) showed that the running-in process is largely completed within the first few contact cycles, corresponding to the number of opposing surface areas seen. Similar findings were shown by Sosa et al. (17) through in-situ profilometer measurement, while Martins et al. (15) found the first stage at increased load also featured an associated running-in effect. Conversely, other methods suggested to determine the conclusion of running-in would require significantly more cycles—for example, the establishment of a steady state for friction and wear-rate (18) or contact voltage reaching 90% of for the applied voltage, thus indicating total separation of the surfaces. (19) Hansen et al. (7) found that rougher surfaces required more load cycles to complete the running-in process.

This paper concerns the influence of pressure (P), slide-roll ratio (SRR), and entrainment velocity (U), on surface

parameters through running-in. The data in this paper were obtained from the early stages of a sequence of endurance tests designed to investigate micropitting initiation. That work is reported in detail in Part Two of this paper, whereas this paper presents in detail a systematic experimental evaluation of contact conditions on running-in behavior, using a full-factorial experimental design, that is not yet available in the literature.

## Method

Testing was performed using a twin-disk rig, an established method of testing in EHL conditions representative of gear contacts without the complex transient kinematics of real gear tests. A schematic of this test rig is shown in Fig. 1. In this test rig a three-phase electric motor is connected to the fast shaft by a speed-increasing gear pair. The fast shaft is then separately geared to the slow shaft by a speed-decreasing gearbox that imparts a chosen SRR to the contact. Three pairs of gears with different transmission ratios (henceforth referred to as the “SRR gears”) were used in this work to give SRRs of 0.25, 0.375, and 0.5.

Both shafts were supported by two bearings and fitted using an arrangement of flexible couplings to ensure the shafts remained parallel throughout the test. The slow shaft bearings were mounted in a pivoting housing, allowing the

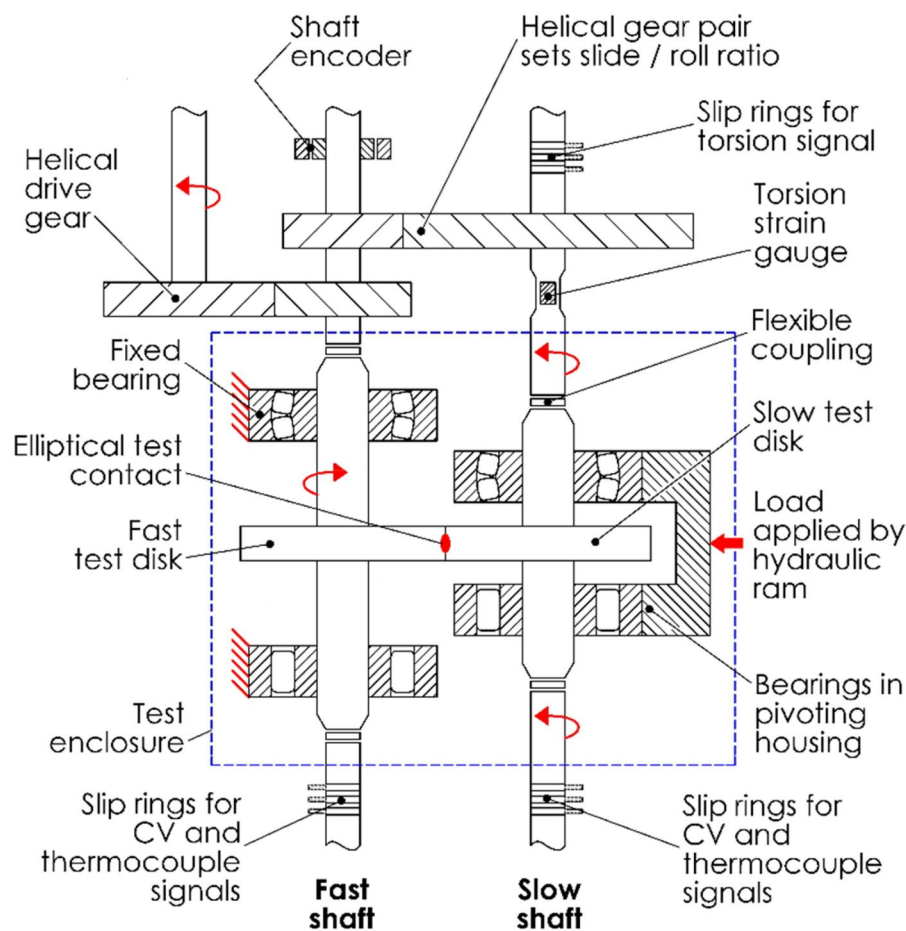


**Figure 1.** Schematic of the test head of the twin disk rig. Figure adapted from Hutt, S., Clarke, A., and Evans, H. P. (2018), “Generation of Acoustic Emission from the Running-In and Subsequent Micropitting of a Mixed-Elastohydrodynamic Contact,” *Tribology International*, 119, pp 270–280.

distance between the disks to vary as necessary. Load was applied to the slow disk via the pivoting housing by a hydraulic ram. A load cell was used to measure the applied force, with the load gradually ramped to the target value at the start of each test (the test commenced at the point the target value was reached).

Thermocouples embedded some 3 mm beneath the disk surface, on the disk centerline, were used to record and monitor disk temperature. Additionally, the slow shaft was electrically isolated from the rest of the rig, allowing contact voltage (CV) between the disks to be measured (a full description of the CV system can be found in (20)). Slip rings for the fast and slow shafts allowed the thermocouple and CV signals to be passed to the computer. A torsion strain gauge was fitted to the shaft connecting the slow shaft to its driving gear, which allowed a measurement of the contact friction to be obtained.

The test disks were made of EN36 steel with a mean hardness of 714 Hv. The disks were 76.2 mm in diameter, with a crown of radius 304.8 mm. This produced an elliptical contact with an aspect ratio of 4:1, with the minor axis of the ellipse aligned to the entrainment direction. To accurately represent gear teeth with transverse roughness, the disks were ground using the arrangement shown in Fig. 2, in which the disk was ground on the inside of a conical grinding wheel. This both produced an approximately transverse finish (a mild “sweep” effect remains) and imparted the desired crown to the disks. A target Ra of  $0.4 \mu\text{m}$  was selected to be representative of gear roughness however due to the complexity of grinding to an exact finish a margin of error was allowed. The disks used therefore had a mean Ra =  $0.42 \mu\text{m}$ , with all values between  $0.37 \mu\text{m}$  and  $0.46 \mu\text{m}$ . Both fast and slow surface disks were selected at random from the same pool for each test.

Two Vickers hardness indents were made in the disk surface outside of the contact area to serve as reference points

for measurement, as well as an engraved reference line on the outside face of the disk.

To systematically investigate the influence of P, SRR, and U on the contact, a factorial experimental design was employed. This arrangement allows the effects of each variable and each interaction between variables to be assessed in the minimum number of tests. Using a high and low setting for each variable requires a total of eight tests.

An additional “center point” test in which all variables were set halfway between the high and low settings was also performed to establish whether the effects seen were linear or nonlinear in nature.

Table 1 shows the conditions applied for each test in the experimental program. For all tests, the lubricating oil was OEP-80, (21) supplied to the contact area at  $80^\circ\text{C}$ . A number of scoping experiments were conducted to establish parameters for the tests that would produce challenging conditions without resulting in test failure. For example, SRR of 0.75 and disk roughness of  $R_a = 0.6 \mu\text{m}$  were both shown to induce scuffing failure during the running-in process; therefore, less challenging conditions were adopted.

Table 1 also shows the specific film thicknesses ( $\Lambda$  ratios) calculated using the surface roughness measurements taken before and after the running-in tests. It can be seen that the effect of running-in is to increase the specific film thickness, due to the removal of the most aggressive asperity features reducing the overall composite surface roughness. Although the lowest values of  $\Lambda$  seen in these tests (around 0.2) are indicative of very heavily mixed-lubrication conditions or even boundary lubrication, it has previously been shown that partial EHL films persist in these conditions. For example, the mixed lubrication simulations of Sharif and coworkers (4) showed the effects of decreasing  $\Lambda$  on P and film thickness for rough surfaces similar to those studied in this paper, under operating conditions typical of heavily

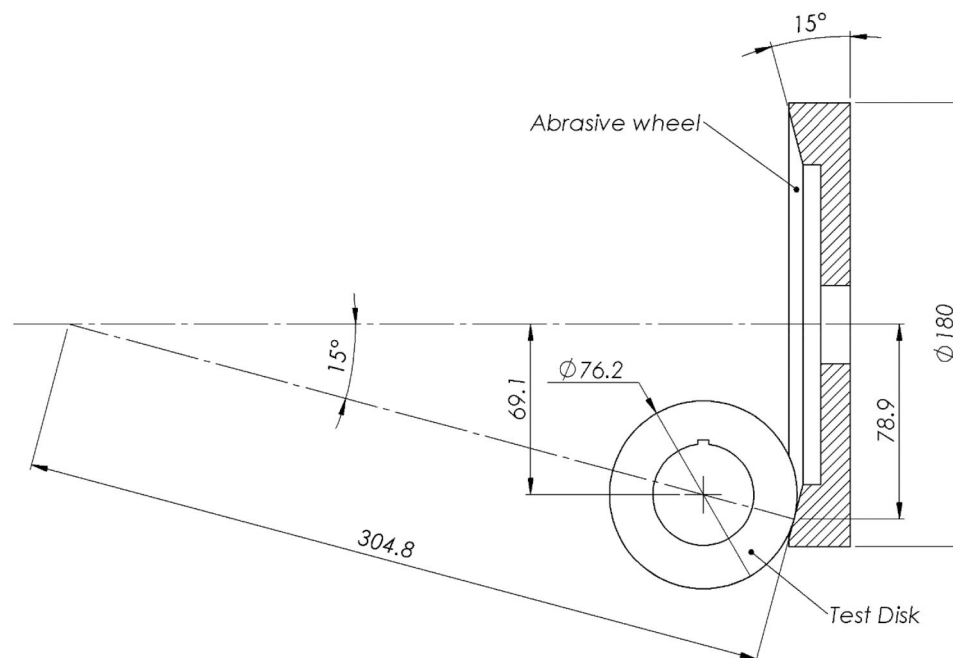


Figure 2. The disk grinding arrangement used to produce a transversely ground finish around the circumference of the disk.

**Table 1.** Test conditions, presented in chronological order.

Test	Max Pressure /GPa	SRR	Entrainment Velocity / $\text{ms}^{-1}$	Fast Disk Ra / $\mu\text{m}$	Slow Disk Ra / $\mu\text{m}$	Specific Film Thickness $\Lambda$ , at test start	Specific Film Thickness $\Lambda$ , at test end
Test 1	1.6	0.500	4	0.42	0.43	0.18	0.23
Test 2	1.6	0.500	2	0.39	0.40	0.15	0.19
Test 3	1.6	0.250	2	0.37	0.44	0.19	0.24
Test 4	1.2	0.500	2	0.41	0.41	0.22	0.27
Test 5	1.2	0.250	4	0.41	0.38	0.39	0.44
Center point	1.4	0.375	3	0.46	0.41	0.22	0.27
Test 6	1.6	0.250	4	0.45	0.46	0.25	0.29
Test 7	1.2	0.250	2	0.45	0.46	0.22	0.26
Test 8	1.2	0.500	4	0.43	0.46	0.31	0.35

Abbreviations: SRR, slide-roll ratio.

loaded power-transmission gearing. They found that even when  $\Lambda = 0.1$ , load carrying EHL films were present over significant parts of the contact, together with localized direct asperity contacts.

In factorial tests, the influence of individual variables (e.g.,  $P$ ) may be assessed by averaging the results of the desired output (e.g., Ra) of tests where that variable is low, and separately averaging the output where that variable is high. Assuming linearity in all responses, the influence of other factors (e.g., SRR and  $U$ , and interaction effects) will cancel out in the averaging process. Plotting these two points on a graph of variable versus output (Ra in this example) shows the effect on Ra of changing that variable from the low to high setting.

Finding the effect of an interaction between multiple variables is similar, however the interaction “high” and “low” settings must first be established. A two-factor interaction is present where the change in one variable causes a subsequent change in the effect of another variable. In any instance where both interacting variables are set high or both set low, this would be considered the “high” setting. Where one is low and the other high, this constitutes the “low” setting. Again, averaging high- and low-test results enables the effect of the interaction to be identified.

An alternative way of considering multifactor interactions is to adopt a notation wherein if a variable is “high” during a test then it is noted as 1, and if low,  $-1$ . For each test, multiplying these notations for all factors involved in an interaction together will yield a 1 or  $-1$  indicating whether that test has a “high” or “low” interaction setting. This approach continues to work easily where there are three variables interacting. A three-variable interaction indicates that a change in one variable causes a resultant change in the two-factor interaction effect between the other two variables. Readers unfamiliar with factorial tests may find the resources available at (22,23) helpful in interpretation of factorial test results.

To establish whether there are nonlinear effects present, the center point test may be plotted on the graph of each individual or multi-factor effect. If a straight line between the averaged high and low setting results for a variable or interaction passes through the center point result, it is likely a linear relationship. If it does not, some level of nonlinearity is likely to be present, though the order of nonlinearity

cannot be established from a test program with only high and low settings.

In this work, running-in was considered to have concluded after six thousand fast disk cycles – this allowed sufficient time for the surface to reach a steady state after the initial deformation. (5) This was reached in two test stages, each consisting of three thousand fast disk cycles. The number of cycles experienced by the slow surface during running-in varied dependent on the applied SRR.

Two-dimensional surface profiles were obtained in-situ prior to running and after each test stage using a Taylor Hobson Intra 2 portable profilometer mounted on a manually operated stage. The measuring locations were axially relocated by the following procedure:

- The stylus was located in the approximate center of the disk circumference by eye and lowered into contact.
- The stage was moved axially toward the slip rings using a lead screw until the reading decreased by  $60 \mu\text{m}$  (indicating the disk edge).
- The gauge was then zeroed.
- The stylus was moved to the correct position relative to the disk edge.

For each test, measurements of 12 mm length were made at nine positions including the centerline and four increments of  $\frac{2}{9}b$  each side (where  $b$  is the Hertzian half-dimension perpendicular to the entrainment direction), as shown in Fig. 3.  $\Delta x$ , the spacing of measurement points in the entrainment direction, was  $0.5 \mu\text{m}$ . A gaussian filter with a cutoff wavelength of  $0.8 \text{ mm}$  was applied to each profile to remove the disk form and waviness features not relevant to the contact.

The majority of roughness parameters explored were found according to ISO 4287 using the TalyMap software. All surface parameters considered through running-in are summarized in Table 2.

Bespoke MATLAB code was developed to evaluate the Radius of Curvature, Asperity Height, and Asperity cross-sectional area (CSA) parameters, which fall outside of ISO 4287.

To calculate radius of curvature, asperity tips first had to be identified. To be considered for this analysis the asperity tip was required to be at least  $0.5 \mu\text{m}$  above the mean line of the profile, as these peaks are the most likely to come into

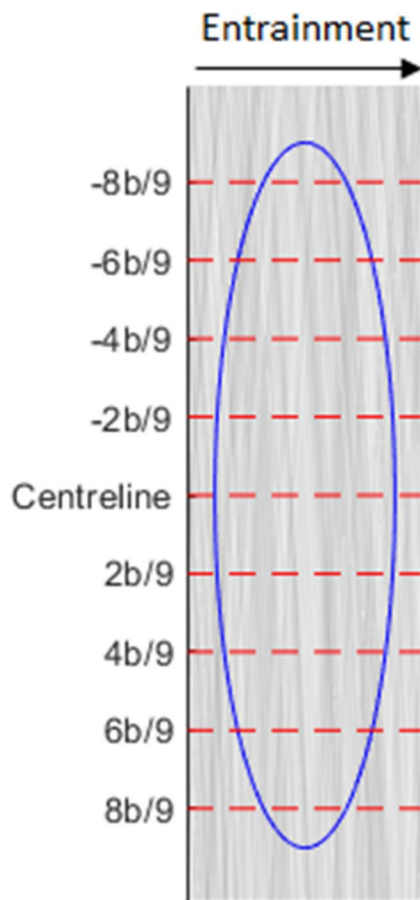


**Figure 3.** Scale illustration of the contact ellipse with measuring positions for two dimensional profiles.

**Table 2.** Roughness and profile parameters used for analysis of running-in.

Roughness	Profile Parameters
Rp	Maximum profile peak height
Rv	Maximum profile valley depth
Rz	Maximum peak to valley height
Rc	Mean height of profile elements
Rt	Total height of the roughness profile
Ra	Arithmetical mean roughness
Rq	Root-mean-square roughness
Radius of Curvature	Radius of curvature of asperity peaks
Asperity Height	Mean height of asperities above the mean line
Asperity CSA	Mean cross-sectional area of asperities above the mean line

Abbreviations: CSA, cross sectional area.

contact and this approach reduced false peak identification. To be valid for consideration, the measurement point was required to be higher than each of its neighbors, each of which was then required to be higher than their remaining neighbor. A five-point mean sagitta length method (24) was employed as illustrated in Fig. 4. For each asperity, two circles were constructed, one passing through the peak and both neighbors to the left, and the other through the peak and both neighbors to the right as in Fig. 4a. The sagittas (S1 and S2 in the figure) were calculated trigonometrically and the mean of these ( $S_{\text{mean}}$ ) was found. The radius of a circle corresponding to that sagitta and  $\Delta x = 0.5 \mu\text{m}$  was then calculated and taken as the radius of curvature of the asperity tip.

The asperity height and asperity CSA were calculated by dividing the profile into elements each containing an

asperity bounded by valleys, as shown in Fig. 5. This was achieved through use of turning points. The asperity height was then determined as the maximum height of the asperity from the mean line (differing from the Rc parameter which is a valley to peak height), while the asperity CSA was calculated as the area bounded by the profile and the mean line. The radius of curvature of asperity tips, asperity height, and asperity CSA considered for each profile were mean values for all asperities considered.

## Results

The first two tests were expected to provoke the most severe conditions in the contact and were intentionally placed at the start of the experimental program as part of a scoping phase. Both tests exhibited unusual mild wear behaviors. In the case of Test 1 (Fig. 6a), this appeared in the form of a continuous, shiny central band on both fast and slow surfaces. For Test 2 (Fig. 6b) a large number of small patched “islands” of wear were produced on the fast and slow surfaces.

Closer inspection showed these regions to contain surface damage reminiscent of micro-scurfs or score marks. These are indicative of a breakdown in lubrication in these regions of the surface. The surface parameters within these regions were shown to differ from the areas that did not encounter wear effects—most notably the radius of curvature of asperities in these regions increased much more than on the rest of the surface. To keep the factorial program analysis valid for the influence of P, SRR, and U on running-in across the tests performed, only profiles which did not pass through worn areas on these surfaces were included in the factorial analysis. No other tests exhibited this wear behavior.

For each test, the surface parameters listed in Table 2 were evaluated for each profile measured on the unrun surface, after three thousand fast disk cycles, and after six thousand fast disk cycles. The mean values for the fast and slow surfaces were then recorded. An example of this is shown in Fig. 7 for the center point test. It is clear in this figure that the majority of change occurred during the first test stage. Most parameters remained essentially unchanged through the second test stage, while a few (for example the fast disk radius of curvature and  $Rv$ ) underwent a much smaller second stage of modification. This behavior was representative of all tests in the program and is consistent with previous observations showing that the main changes during running-in occur rapidly. (5,16).

This conclusion that running-in occurred rapidly is supported by the measured friction and contact voltage values, which stabilized by the end of the first stage (3,000 fast disk cycles) to values shown previously by the authors (5,16) to be consistent with stable surfaces operating in the mixed-lubrication regime. A typical result for contact voltage and friction is shown in Appendix, for Test 4, together with more detailed explanation.

The factorial analysis of the experimental program was completed using the change in value for each parameter between the unrun and run-in states (6,000 fast disk cycles).

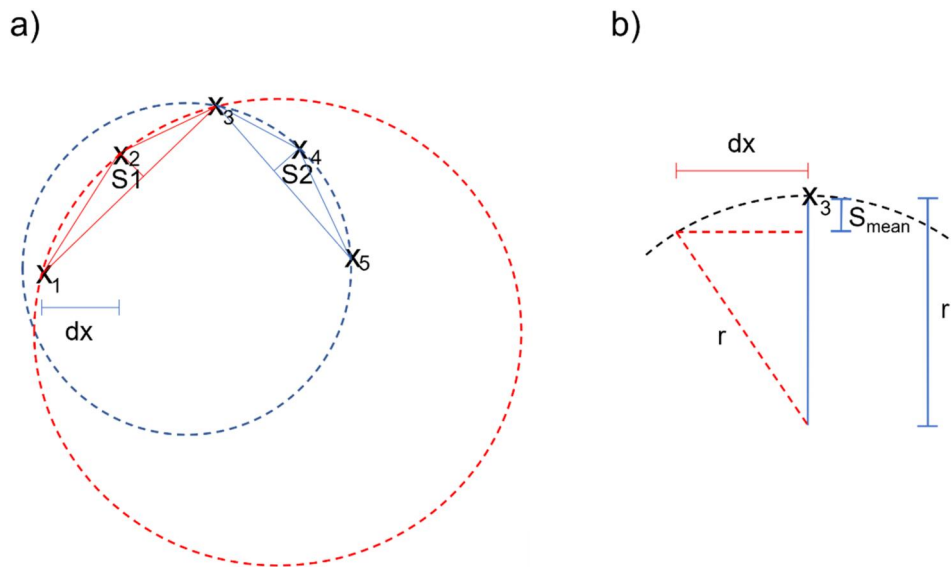


**Figure 4.** Determining radius of curvature of asperity tips. a) construction of two circles from the 5 points at the tip b), determination of the radius of curvature from the mean sagitta.

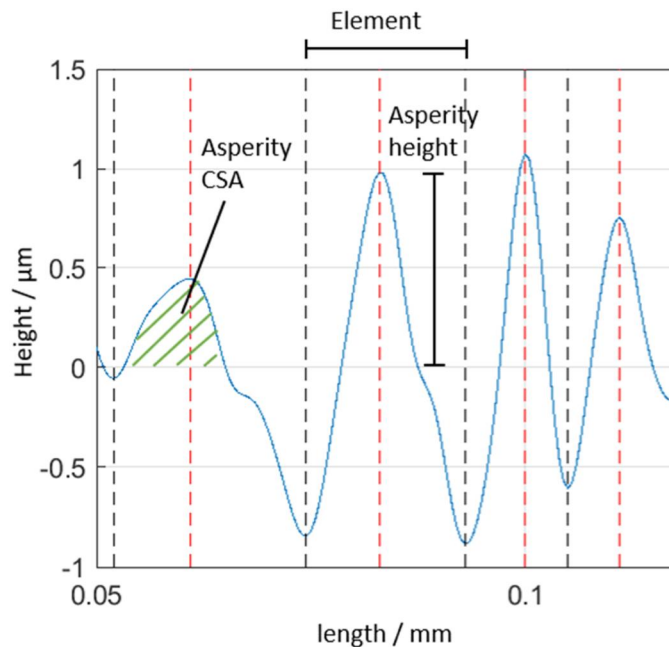


**Figure 5.** Profile section with identified valleys (black dashed lines) and peaks (red dashed lines) indicated. Elements are defined as the sections between two valleys, with asperity height and asperity cross-sectional area (CSA) found as indicated on the figure.

The roughness parameters for each test (as in Fig. 7) are evaluated as the mean for all valid profiles across the disk width.

Table 3 shows the mean surface parameters before and after running for the fast and slow surfaces in each test.

For ease of discussion, the results will be discussed in four groups; general roughness parameters ( $R_a$ ,  $R_q$ ), mean radius of curvature of asperities, extreme roughness parameters ( $R_p$ ,  $R_v$ ,  $R_z$ ,  $R_t$ ), and element-wise parameters ( $R_c$ , mean asperity height, mean asperity CSA).

### General roughness parameters

The main effects on  $R_a$  and  $R_q$ , as assessed by the factorial experiment, can be seen in Fig. 8. The points on each graph are an average—for instance, considering P, at the point at 1.2 GPa, shows the mean change in  $R_a$  or  $R_q$  (as applicable) for the four tests where P was “low,” and correspondingly at 1.6 GPa the point shows the mean change in  $R_a$  or  $R_q$  where the P was “high.” For both  $R_a$  and  $R_q$ , elevated P led to a greater reduction in the value through the course of running-in. SRR also acted to decrease the  $R_a$  and  $R_q$  in all cases. However, the effect of SRR was typically very small—with the notable exception of the fast surface  $R_q$ , for which SRR had the largest influence of all three factors. Across all surfaces, increased U protected the surface and reduced the modification of the  $R_a$  and  $R_q$  through the first two test stages.

Inspection of Fig. 8 shows that, for the  $R_a$ , the center point test result occurred on the line for the fast surface and was very close to the line for the slow surface. This is indicative of linear behavior. The  $R_q$  result in both surfaces was slightly removed from the line, indicating mildly nonlinear behavior.

Two-factor interaction plots for  $R_a$  and  $R_q$  are shown in Fig. 9. In each plot, the change in one parameter is shown on the x-axis (e.g., for the leftmost of the top row in each figure, SRR) while for the remaining parameter (corresponding to the row, from top to bottom P, SRR, and U) the high and low settings are indicated by use of solid or dotted lines respectively. In this way, for the Fast  $R_a$  figure shown at top left the paired squares labeled (a) compare the effects of parameter pair SRR and P. The paired squares labeled (b) compare the effects of parameter pair U and P, and the paired squares labeled (c) compare the effects of parameter pair U and SRR. The color of the lines in each square identifies the line parameter and the coordinates of the  $R_a$  or  $R_q$  points plotted are the average value for the two corresponding tests for each point obtained from Table 3.

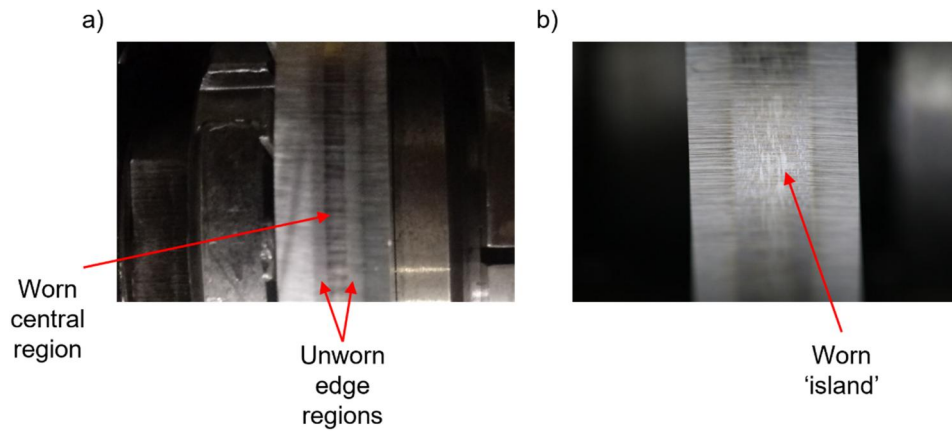


Figure 6. a) Test 1 surface after running-in with worn Central band and unworn regions indicated. b) Test 2 surfaces after running-in with an example wear "island" indicated.

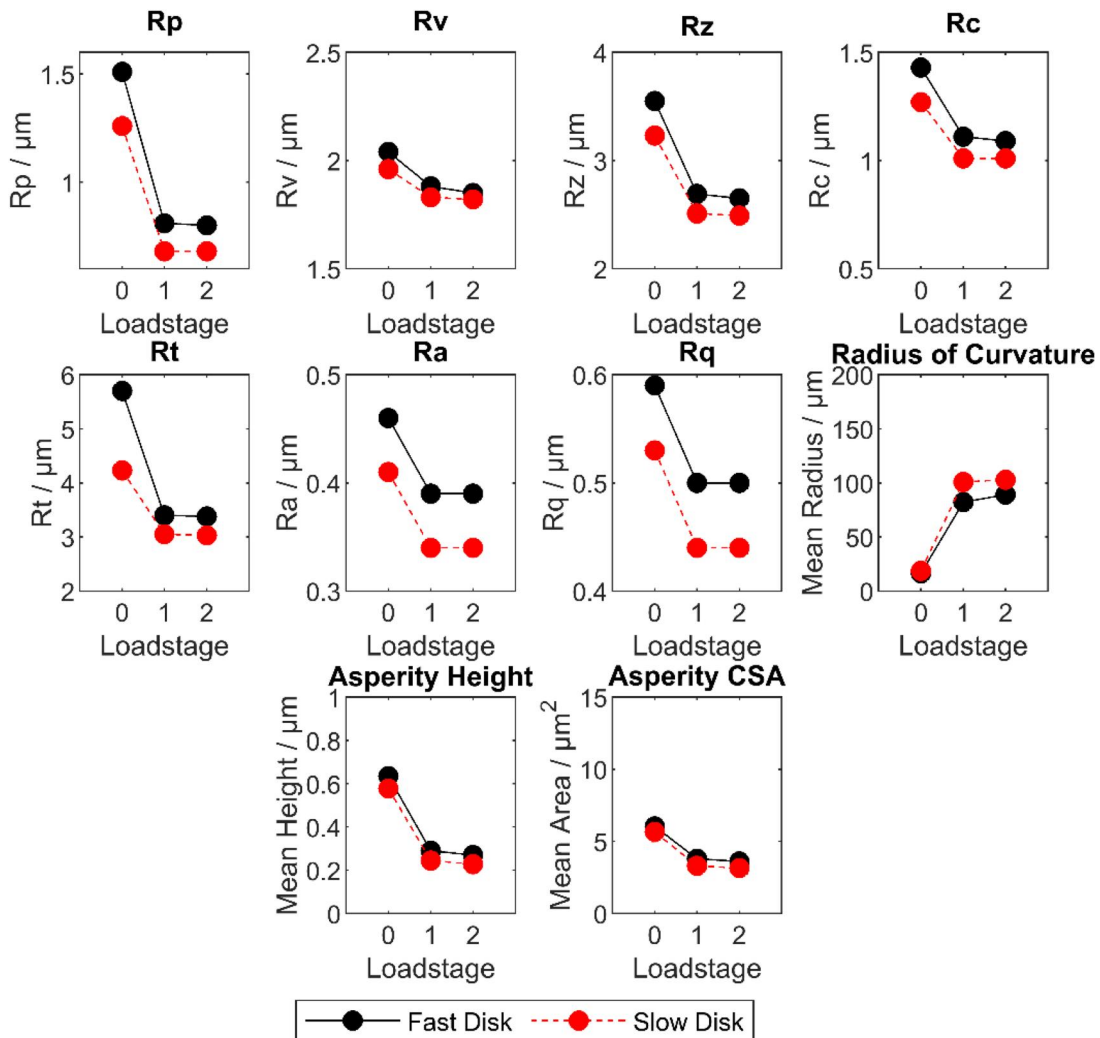


Figure 7. Surface roughness parameters for the fast and slow surfaces of the center point test through running-in from the unrun surface (test stage 0) to the completion of six thousand fast disk cycles (test stage 2).

Where the two lines are parallel, this indicates that there is no interaction effect between the two parameters. Where the angle of the lines changes between the high and low settings, this indicates the presence of an interaction effect. The magnitude of the interaction effect may be assessed by averaging tests in a similar way to single-factor effects.

However, for interaction effects, tests are averaged where both parameters are set high or low together (considered the "high" setting for the interaction), and where one parameter is set high and the other is set low (considered the "low" setting for the interaction). Only one pair of parameters on the fast surface for both Ra and Rq did not exhibit an

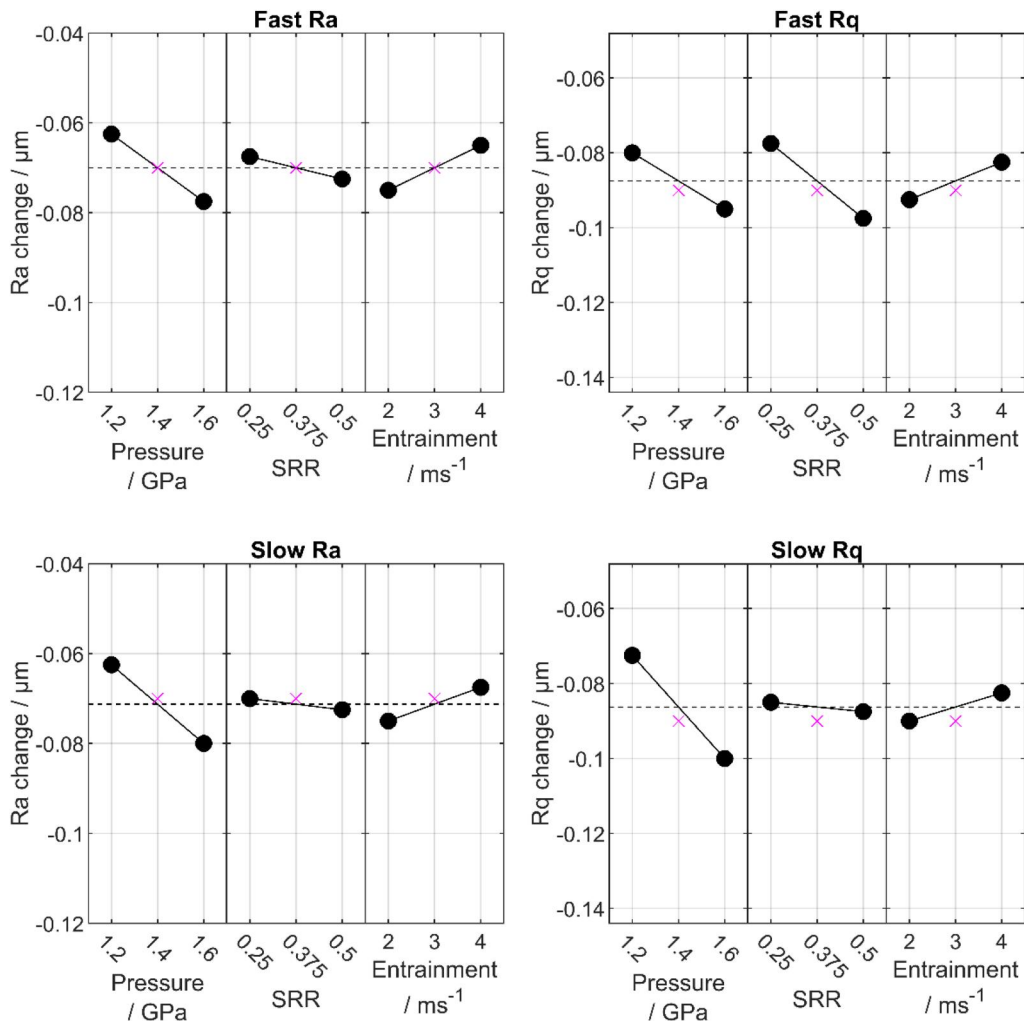
**Table 3.** Surface parameters for the fast and slow surfaces of each test before and after running-in.

		Fast Surface																	
Test		Test 1		Test 2		Test 3		Test 4		Test 5		Centrepoint		Test 6		Test 7		Test 8	
Test stage		0	2	0	2	0	2	0	2	0	2	0	2	0	2	0	2	0	2
Mean Asperity CSA / $\mu\text{m}^2$		5.86	3.43	5.72	2.90	5.29	2.81	5.47	3.31	5.93	4.33	6.03	3.61	6.49	4.35	5.67	3.11	5.75	3.45
Mean Asperity Height / $\mu\text{m}$		0.56	0.22	0.54	0.17	0.55	0.20	0.58	0.26	0.58	0.35	0.63	0.27	0.61	0.32	0.61	0.25	0.59	0.27
Ra / $\mu\text{m}$		0.45	0.36	0.39	0.32	0.37	0.29	0.41	0.34	0.41	0.37	0.46	0.39	0.45	0.38	0.45	0.37	0.43	0.37
Rc / $\mu\text{m}$		1.46	1.11	1.18	0.93	1.14	0.86	1.24	0.98	1.23	1.05	1.43	1.09	1.34	1.11	1.39	1.11	1.28	1.02
Radius of Curvature / $\mu\text{m}$		19.12	96.66	21.09	143.75	18.53	93.30	18.01	88.45	18.62	70.07	16.39	89.09	18.86	79.06	16.44	78.45	18.10	94.16
Rp / $\mu\text{m}$		1.36	0.63	1.14	0.67	1.33	0.65	1.37	0.78	1.22	0.84	1.51	0.80	1.36	0.82	1.42	0.77	1.40	0.73
Rq / $\mu\text{m}$		0.60	0.49	0.49	0.39	0.46	0.37	0.52	0.43	0.51	0.46	0.59	0.50	0.57	0.49	0.57	0.48	0.55	0.46
Rt / $\mu\text{m}$		6.49	3.75	3.27	2.51	3.97	2.60	4.08	3.05	3.88	3.14	5.70	3.38	4.19	3.06	4.33	3.14	3.62	2.62
Rv / $\mu\text{m}$		2.46	2.29	1.50	1.34	1.50	1.37	1.75	1.66	1.48	1.43	2.04	1.85	1.84	1.77	1.91	1.83	1.55	1.48
Rz / $\mu\text{m}$		3.82	2.92	2.63	2.01	2.84	2.02	3.11	2.43	2.70	2.27	3.55	2.65	3.20	2.59	3.33	2.60	2.95	2.21

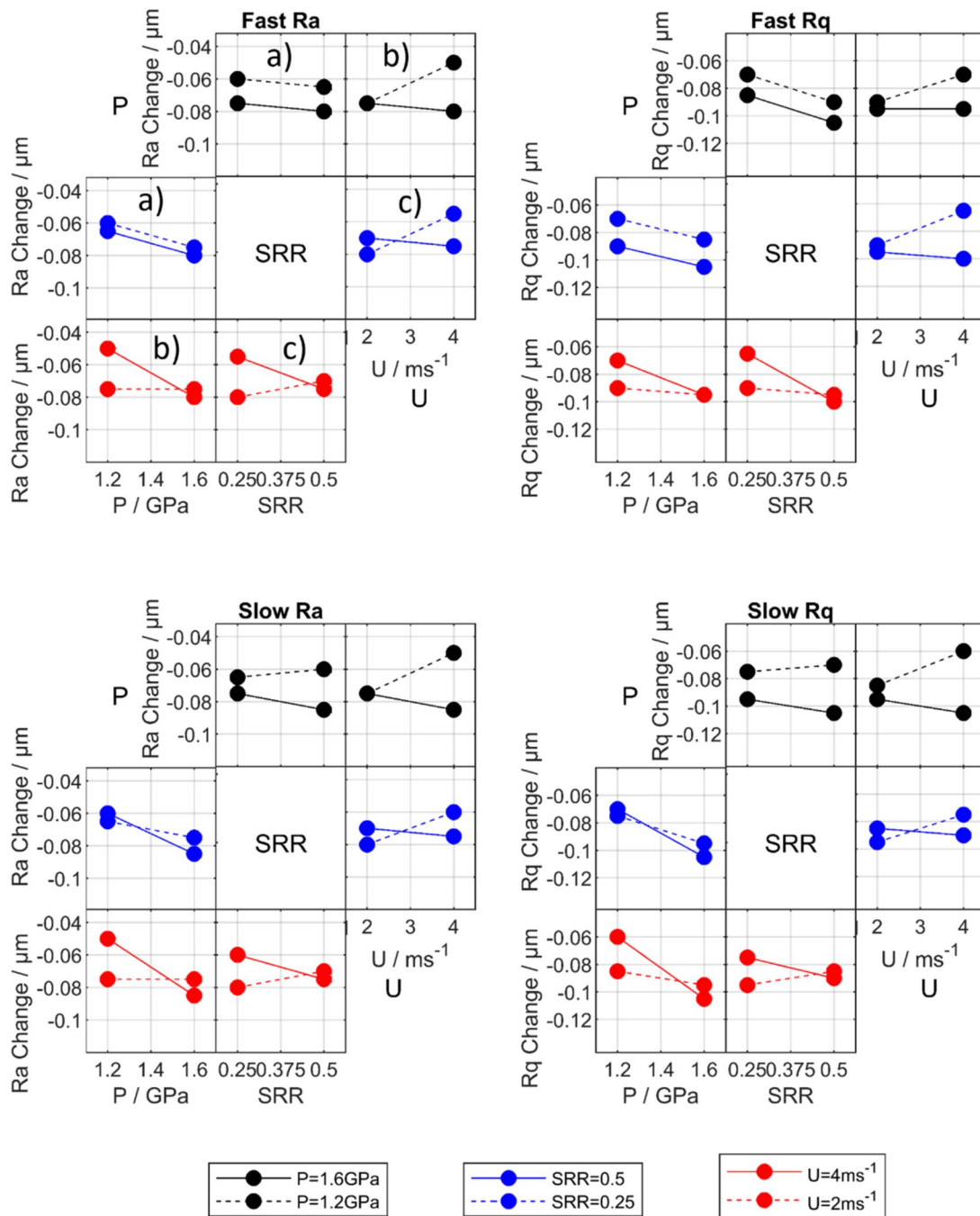
  

		Slow Surface																	
Test		Test 1		Test 2		Test 3		Test 4		Test 5		Centrepoint		Test 6		Test 7		Test 8	
Test stage		0	2	0	2	0	2	0	2	0	2	0	2	0	2	0	2	0	2
Mean Asperity CSA / $\mu\text{m}^2$		4.97	2.53	5.84	3.20	5.80	3.33	5.45	3.25	5.49	3.69	5.65	3.14	6.26	3.75	6.37	3.69	5.83	3.87
Mean Asperity Height / $\mu\text{m}$		0.57	0.19	0.54	0.21	0.61	0.25	0.57	0.25	0.53	0.30	0.58	0.23	0.61	0.28	0.63	0.27	0.61	0.31
Ra / $\mu\text{m}$		0.41	0.31	0.39	0.32	0.44	0.36	0.41	0.34	0.38	0.33	0.41	0.34	0.46	0.39	0.46	0.38	0.46	0.41
Rc / $\mu\text{m}$		1.31	0.99	1.24	0.97	1.33	1.03	1.23	0.99	1.16	0.95	1.27	1.01	1.40	1.13	1.39	1.09	1.40	1.19
Radius of Curvature / $\mu\text{m}$		16.05	93.24	21.80	112.60	16.70	76.41	17.41	82.28	20.37	74.40	18.63	102.90	18.18	67.99	17.28	69.95	16.97	63.58
Rp / $\mu\text{m}$		1.42	0.59	1.17	0.65	1.38	0.76	1.25	0.72	1.22	0.72	1.26	0.68	1.29	0.75	1.48	0.78	1.28	0.85
Rq / $\mu\text{m}$		0.54	0.42	0.49	0.40	0.55	0.45	0.52	0.44	0.48	0.42	0.53	0.44	0.59	0.50	0.58	0.49	0.58	0.52
Rt / $\mu\text{m}$		5.21	3.37	4.41	2.74	4.15	2.76	3.94	2.91	3.91	2.88	4.23	3.03	4.64	3.22	4.57	2.95	4.24	3.45
Rv / $\mu\text{m}$		2.36	2.14	1.56	1.47	1.72	1.56	1.71	1.62	1.67	1.57	1.96	1.82	2.12	2.02	1.79	1.66	2.01	1.88
Rz / $\mu\text{m}$		3.78	2.73	2.73	2.12	3.10	2.32	2.95	2.34	2.89	2.28	3.23	2.49	3.41	2.76	3.27	2.44	3.29	2.73

Abbreviations: CSA, cross sectional area.



**Figure 8.** Main effects of pressure (P), slide-roll ratio (SRR), and entrainment (U) on the Ra and Rq roughness parameters of the fast and slow surfaces. In each case, the cross indicates the result of the center point test, while the dashed line indicates the mean value for all tests.



**Figure 9.** Two-factor interaction plots between pressure (P), slide-roll ratio (SRR), and entrainment (U) for the Ra and Rq roughness parameters on the fast and slow surfaces.

interaction; that being the P-SRR pair. All other interactions were very similar on both surfaces for Ra and Rq. Increased U was shown to protect the surface more effectively when P and/or SRR were low than when they were high. On the slow surface P and SRR interacted strongly in comparison to the lack of interaction on the fast surface.

It should be noted that comparing the angles between lines as an indicator of levels of interaction is only valid when comparing plots showing the same parameters. This is because the units of each parameter are different, and therefore the same angle between different pairs of lines representing different parameters does not necessarily indicate the same level of interaction.

**Figure 10** shows the interactions between P and SRR separately at high and low entrainment velocities, used to identify the presence or absence of three-factor interaction effects. If the interaction between P and SRR (i.e., the relative angle between the two lines, as per the two-factor effect graphs seen previously) is inconsistent when assessed at high and low U, then a three-factor interaction effect is present. For example, for the fast surface Ra lines are parallel at both high and low U; therefore, no three factor effect is present. For Rq on both surfaces, and for the Slow surface Ra, the angle between the lines differs at high and low U. Three-factor interactions are therefore present for the slow surface Ra and for Rq on both surfaces. It should be noted

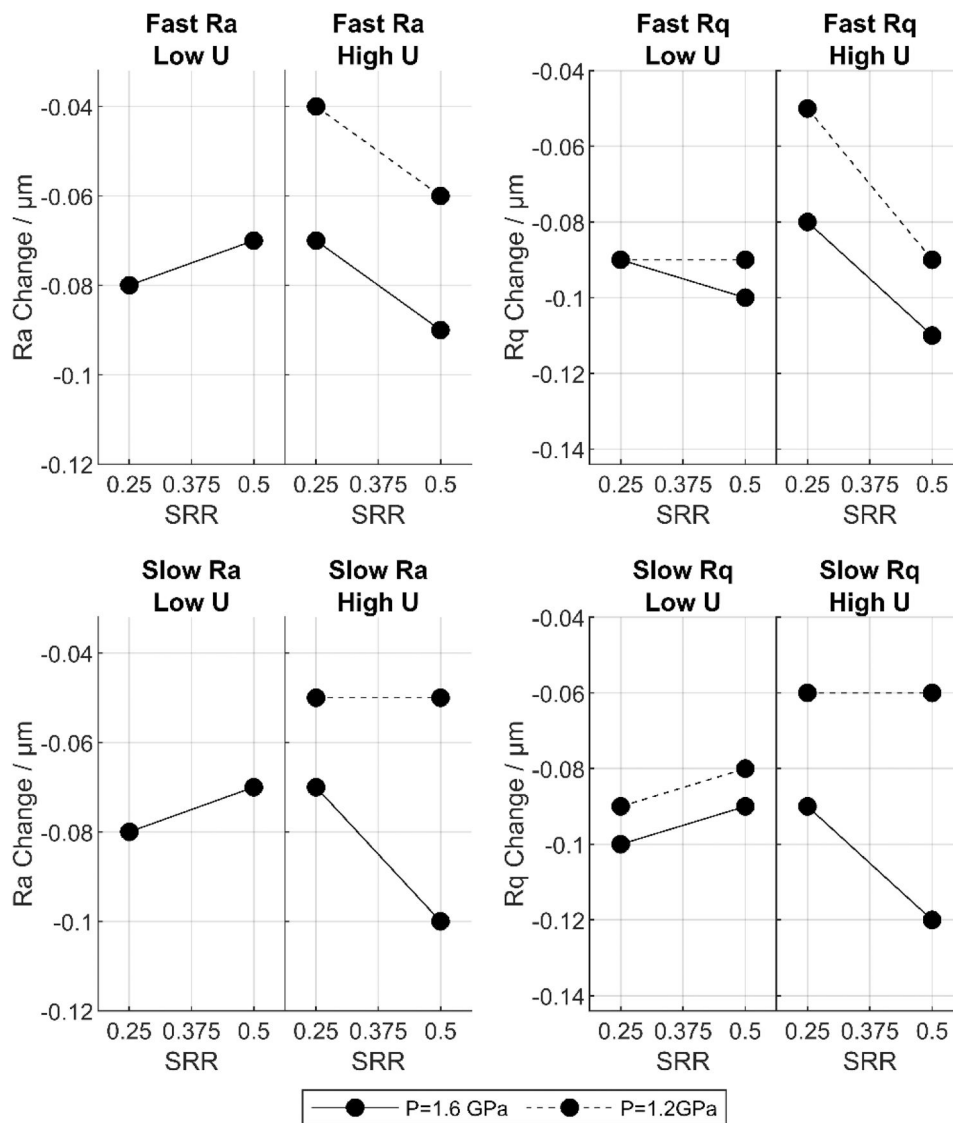


Figure 10. The pressure (P) and slide-roll ratio (SRR) interactions at low and high entrainment (U) for Ra and Rq on the fast and slow surfaces.

that, in Fig. 10, for the plots of fast and slow disk Ra change at low U, the high and low P lines are coincident with each other.

### Radius of curvature of asperities

The main effects on the radius of curvature of asperities can be seen in Fig. 11. The P increased the radius of curvature on both fast and slow surfaces, as did SRR. Again, increasing U provided a protective effect and preserved the asperity tips. All effects were stronger on the fast surface than the slow, particularly in the case of SRR. While the center point result indicated linear behavior on the fast surface, the center point result was significantly removed from the line for the slow surface results. This indicates very strongly nonlinear behavior on the slow surface.

The two-factor interaction plots for the mean radius of curvature of asperities are shown in Fig. 12. Interactions between P and SRR were observed for fast and slow surfaces. The change in P or SRR had a much more significant

effect when the other variable was also set high. On the slow surface, only the “both high” condition for P and SRR was shown to have a significant influence, while all other configurations gave the same average effect.

On the slow surface, P and U did not interact, while on the fast surface high U produced a smaller change in radius as P was increased, compared to the larger change in radius seen at low U when P was increased. Conversely, while minimal interaction was observed between U and SRR on the fast surface, on the slow surface high U was shown to have a stronger protective effect when SRR was high.

Three-factor effects were also observed on both surfaces for the mean radius of curvature of asperities, as shown in Fig. 13.

### Extreme roughness parameters

The extreme roughness parameters as grouped here each reflect the highest or lowest of the points on the surface, or some measurement of the height change between these

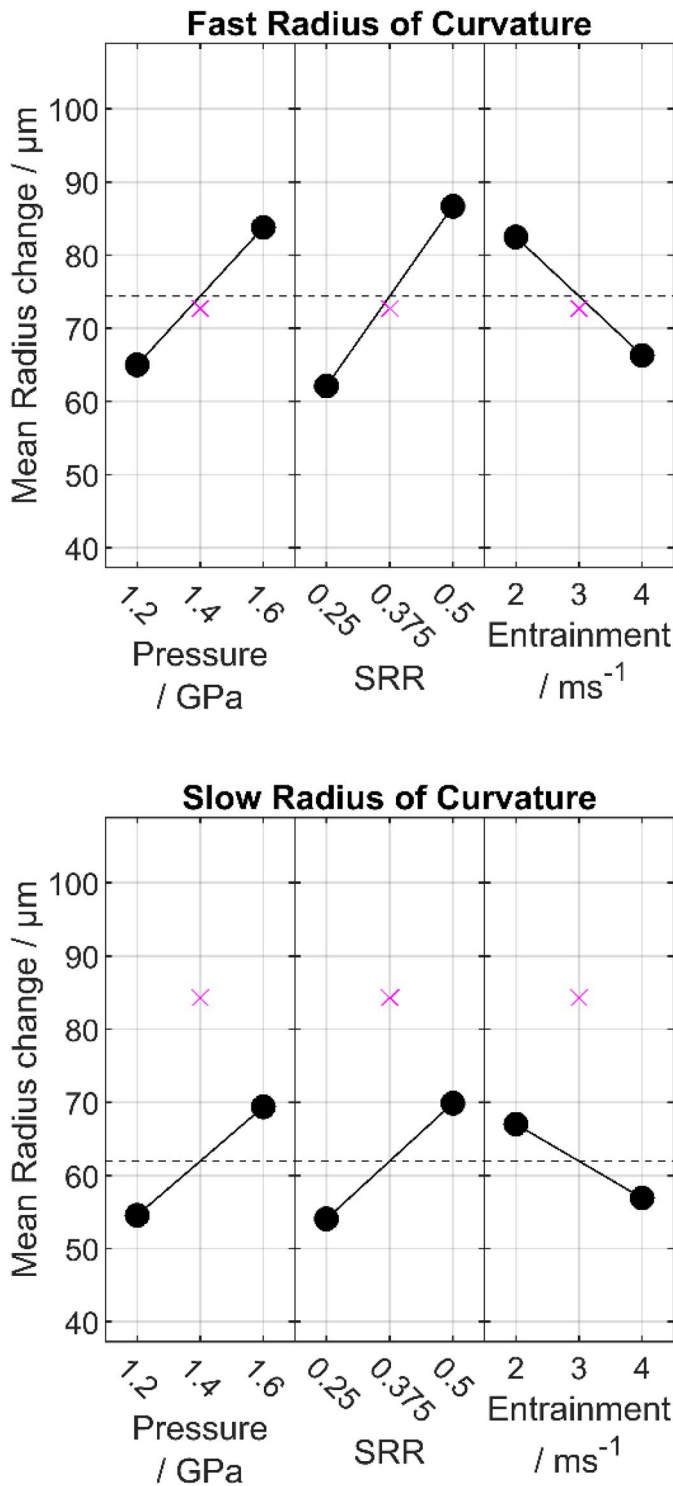


**Figure 11.** Main effects of pressure (P), slide-roll ratio (SRR), and entrainment (U) on the radius of curvature of asperities.

points. The  $R_t$  parameter, which reflects the difference in height between the single highest and lowest points in the measured profile, was quickly seen to be an unreliable measure of the running-in process. The change in  $R_t$  was found to be less a function of the running-in but more heavily dependent on the height of an individual roughness peak in the unrun surface—and to what extent that peak was an outlier. Because of this, the  $R_t$  parameter will not be discussed further, but is included in the summary of results.

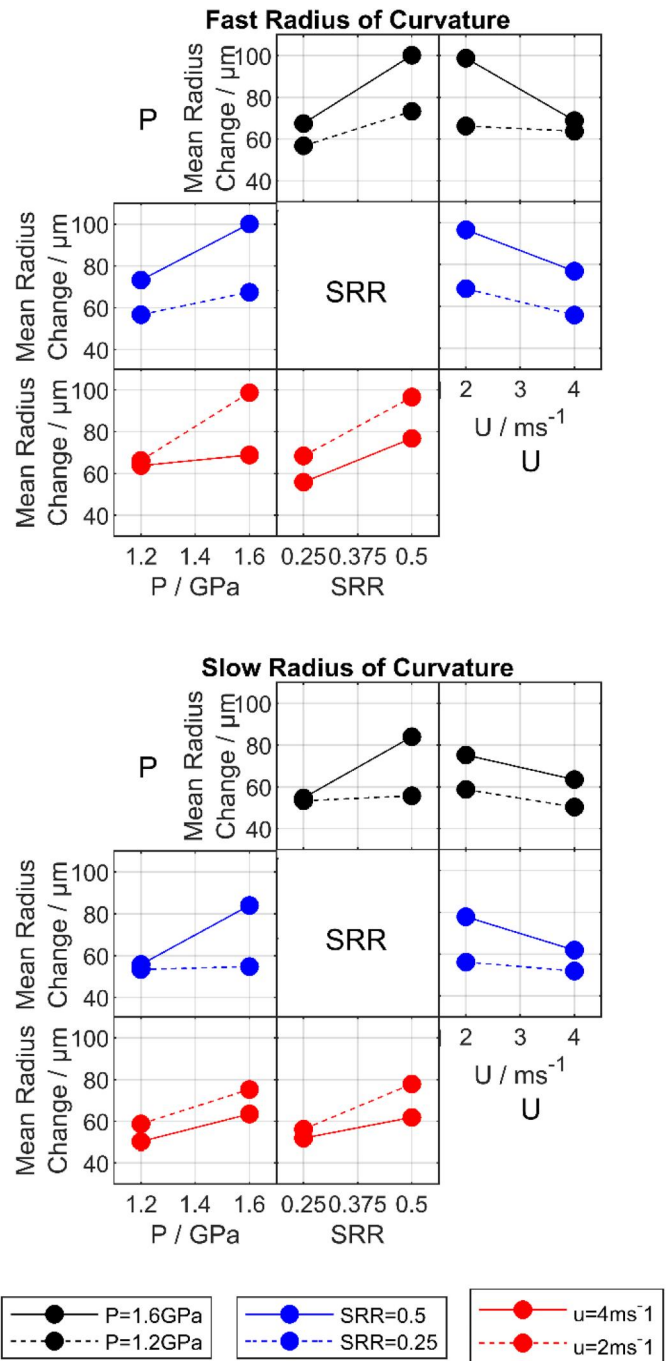


**Figure 12.** Two-factor interaction plots between pressure (P), slide-roll ratio (SRR), and entrainment (U) for the mean radius of curvature of asperities on the fast and slow surfaces.

The main effects for the three remaining extreme roughness parameters are shown in Fig. 14. The effects on  $R_p$  and  $R_z$  match very closely, although the magnitude of effects on  $R_z$  is slightly larger. On the fast surface, both P and SRR induced a decrease in  $R_p$  and  $R_z$ , while U exhibited a very small protective effect. On the slow surface, only P exhibited a significant influence. As might be expected, the difference between  $R_p$  and  $R_z$  values is accounted for by the effects on  $R_v$  (note the much finer scale for  $R_v$  in Fig 14). Fast surface  $R_v$  was decreased by P and SRR, while U opposed this decrease. For the slow surface, increasing any of the three factors acted to decrease  $R_v$ .

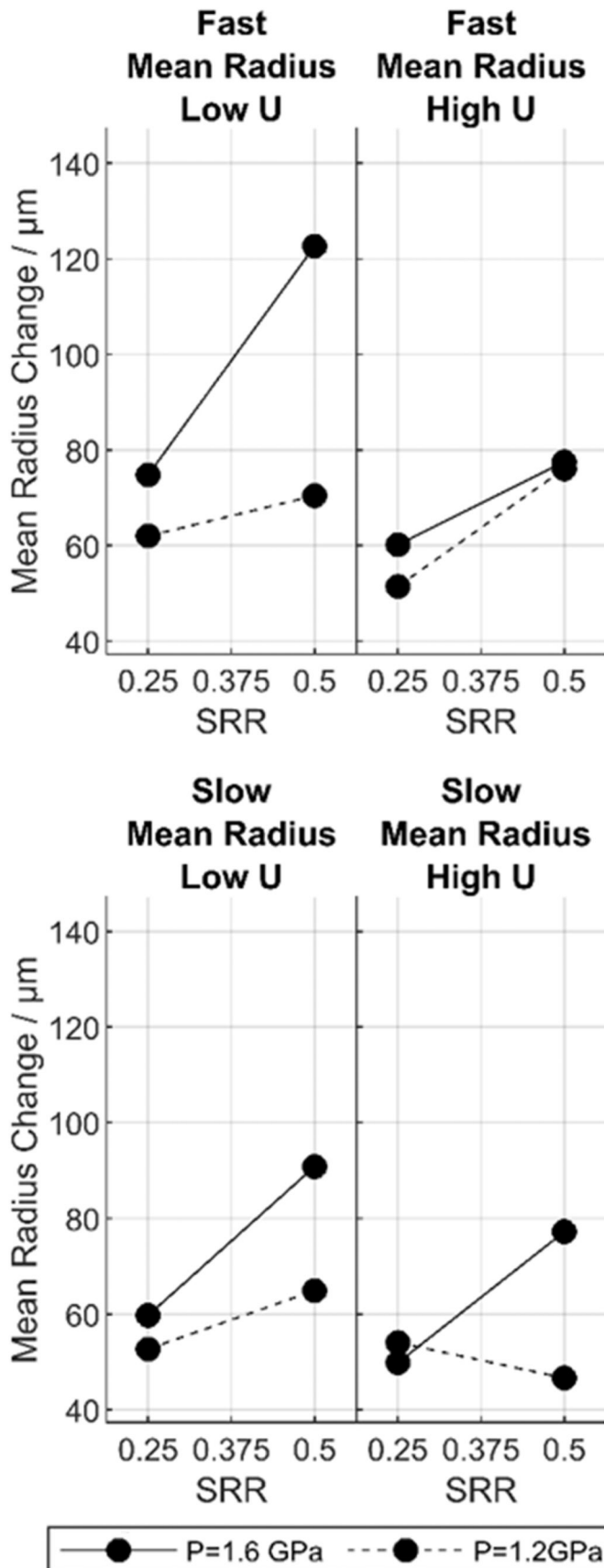


Figure 13. The pressure (P) and slide-roll ratio (SRR) interactions at low and high entrainment (U) for mean radius of curvature of asperities on the fast and slow surfaces.

The matching behaviors between Rp and Rz main effects also applied for the two- and three-factor interaction effects observed; as a result, the effect on Rp shown in Fig. 15 is representative of both parameters. Two-factor interactions were observed between all three factors for Rp (and, hence, also Rz). When U and SRR or U and P were both at the same setting (i.e., both high or both low) then a greater reduction in Rp was observed. The P-SRR interaction effect on Rp differed between the fast and slow surfaces, with the interaction effect increasing or decreasing Rp depending on the surface in question.

For Rv, only the relationship between P and U on the slow surface showed no interaction. On both surfaces, P was observed to have a greater Rv-reducing influence when SRR was high, and a greater influence from SRR was seen when P was high. The interaction between SRR and U differed between surfaces; whereas, increases in SRR at low U caused a small decrease in Rv on the fast surface, and it opposed the decrease in Rv on the slow surface.

Three-factor interactions were present for both Rp and Rv on both surfaces, as can be seen from the change in the P-SRR two-factor interactions at low and high U shown in Fig. 16.

#### Element-Wise parameters

The main effects on each of the element-wise parameters are shown in Fig. 17. For the fast surface across all variables, the effects were very similar. Both P and SRR showed height- and CSA- decreasing effects when they were increased, while increased U again exhibited a protective effect. For mean asperity height and mean CSA, the entrainment effect was the strongest of the three effects; however, it was much smaller for Rc. This may be related to influence of U on the mean-line, as Rc is the only parameter that is not measured relative to the mean line.

On the slow surface, P again reduced the value of the parameters while U opposed this reduction. SRR on the slow surface, however, showed minimal influence for all three parameters. Only the slow surface Rc appeared to show linear behavior.

Two-factor effects for element-wise parameters are shown in Fig. 18. The two-factor effects for mean asperity height and mean asperity CSA were extremely similar; as a result, of these two parameters, only mean asperity height is shown for simplicity. A significant P-SRR interaction was only seen for the slow surface Rc, while the all other two-factor interactions were observed for Rc, mean asperity height, and mean asperity CSA.

Three-factor interactions were observed for all three variables. Again, the mean asperity CSA result closely matched the behavior of the mean asperity height; therefore, only the latter is shown in Fig. 19 alongside the Rc.

The strengths of main and interaction effects for the factors and settings selected are summarized in Table 4, which indicates the magnitude of the change in each surface roughness parameter caused by going from low to high values of the three variables investigated (or combinations of

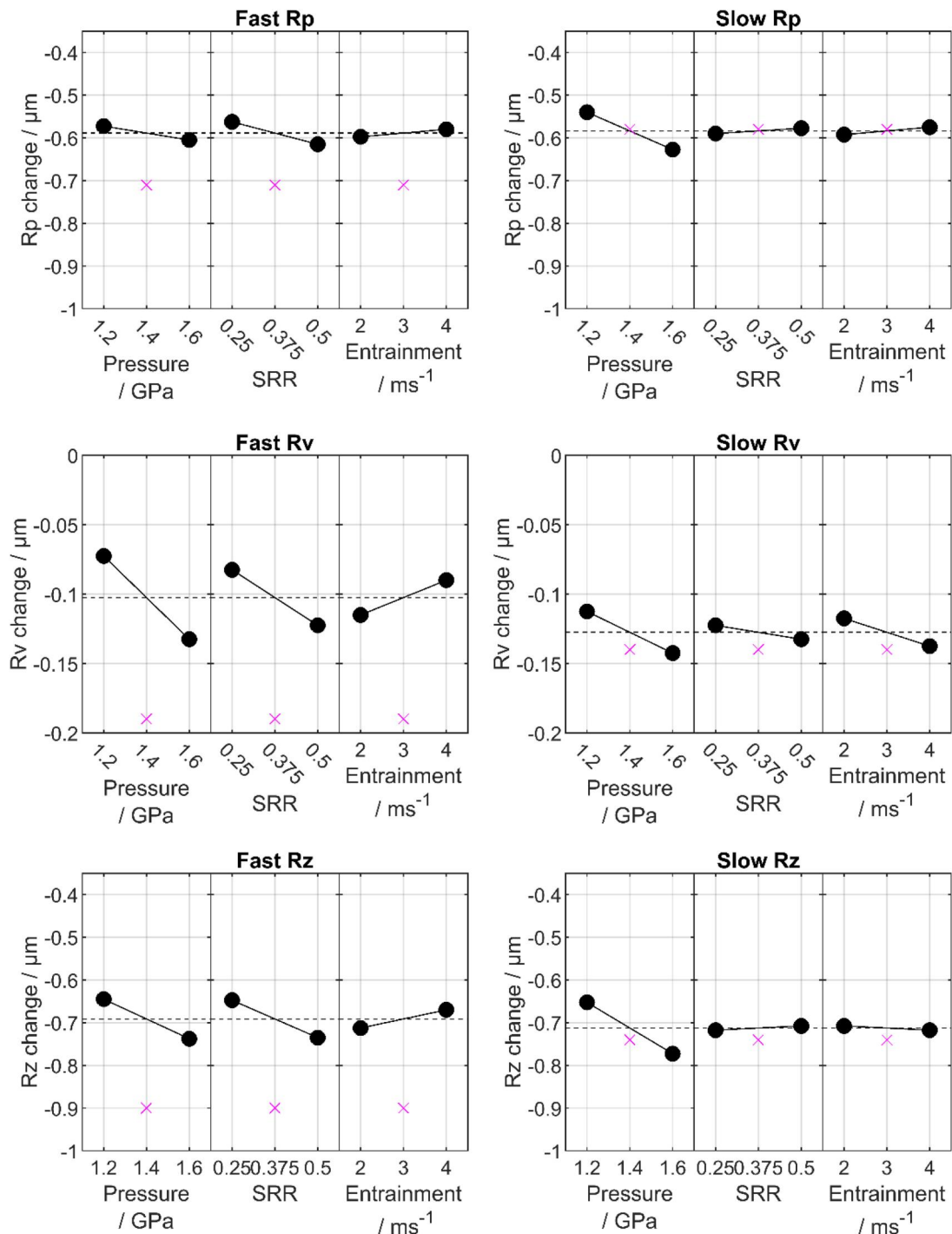


**Figure 14.** Main effects of pressure (P), slide-roll ratio (SRR), and entrainment (U) on Rp, Rv, and Rz for the fast and slow surfaces. Note the finer vertical axis scale for Rv.

these three variables). The normalized effect of each factor or multi-factor interaction on each parameter (normalized against the largest magnitude effect for that parameter across both fast and slow surfaces) is shown in brackets below the absolute effect.

## Discussion

It is clear from the aforementioned results that P, SRR, and U have both individual and combined influences on the surface topography through running-in.

The effect of P was universal across the parameters considered on both disks. In all cases, P increased the magnitude of the overall change recorded, increasing radius of curvature through flattening the surface, but otherwise decreasing the value of all other roughness parameters through running-in. This outcome was largely expected as P increases the amount of plastic deformation induced in asperities, and also increases frictional effects which consequently increases the temperature, thins the lubricant film and encourages abrasive wear, and aligns with the work of Li and Kahraman (25) and Mallipeddi et al. (26) which both

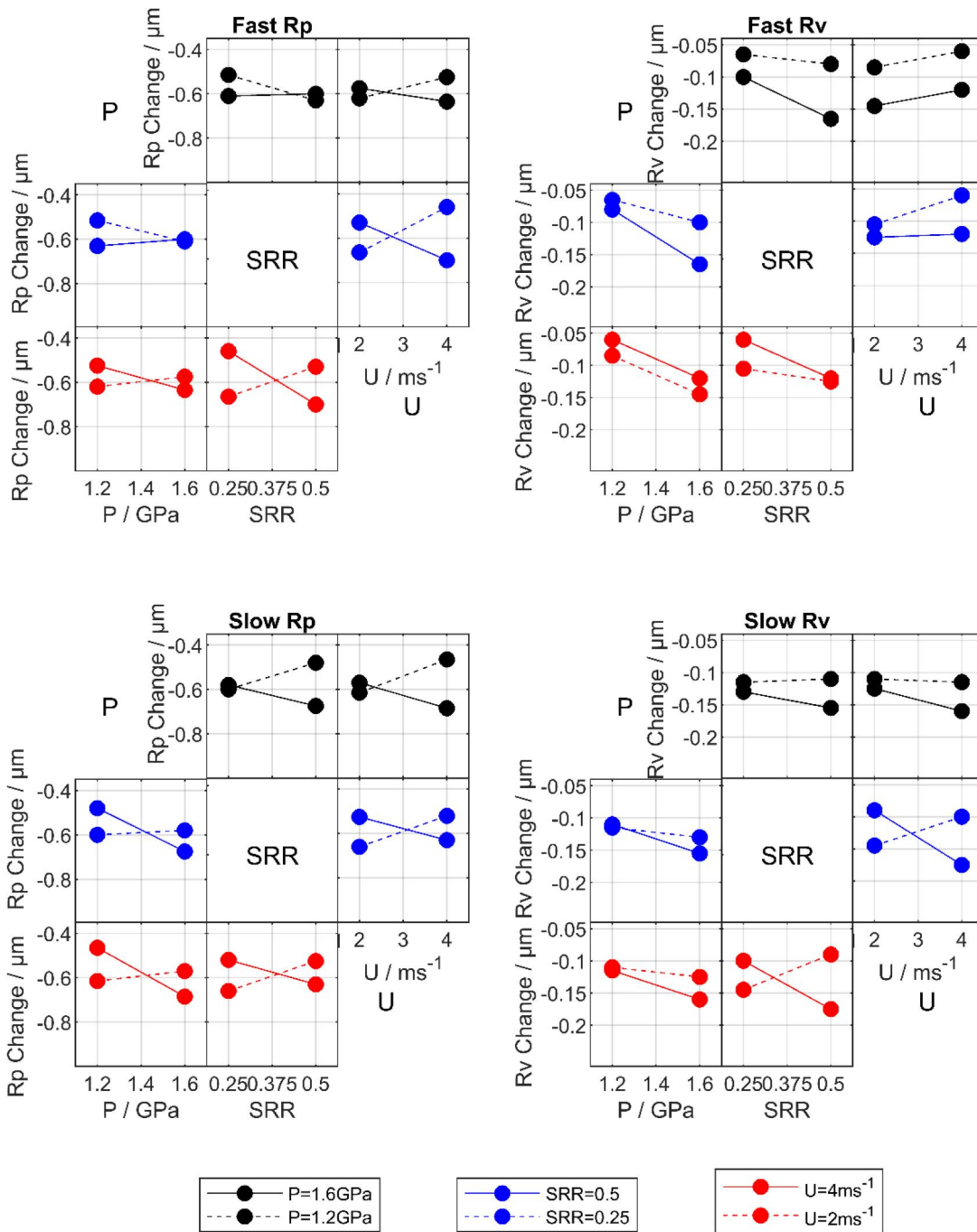


Figure 15. Two-factor interaction plots between pressure (P), slide-roll ratio (SRR), and entrainment (U) for Rp and Rv on the fast and slow surfaces.

observed that increased loads polished or smoothed asperities during running-in.

The effect of U however typically reduced the magnitude of change in parameters during the initial stages of operation—that is, it typically acted in the opposite sense to the effects of P and/or SRR. Entrainment velocity has received a minimal amount of attention in literature, its primary effect being as a dominant factor in the generation of a lubricant film. The production of a thicker lubricant films at higher entrainment velocities is almost certainly the mechanism by which this protective effect is achieved. The production of a thicker lubricant film increases the specific film thickness  $\Lambda$ , which has received more attention particularly in terms of

the subsequent wear and fatigue. It is tempting therefore to try and assess the effect of  $\Lambda$  on the surface modification in place of entrainment velocity; however, this has been resisted in this case. As multiple variables are changing simultaneously it is not possible to isolate and understand each contributing factor to the  $\Lambda$  ratio, and as has been argued previously (27) the impact of a given  $\Lambda$  value on surface modification is highly dependent on the factors which produced it and may not always be simply reduced to a single number.

U provided less effective protection for the “extreme parameters” group. For Rp and Rz this is easily explained: while the increased lubricant film thickness is able to protect

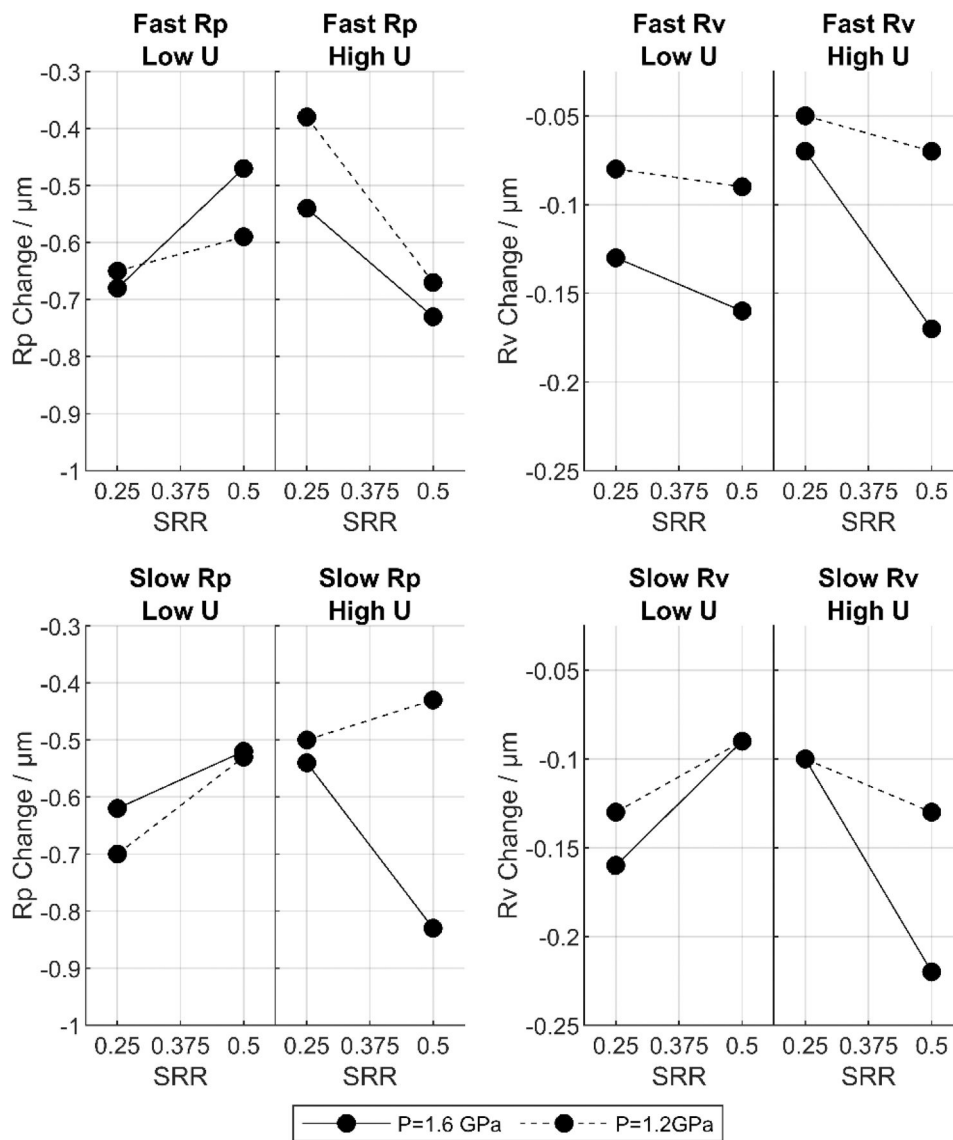


**Figure 16.** The pressure (P) and slide-roll ratio (SRR) interactions at low and high entrainment (U) for Rp and Rv on the fast and slow surfaces.

more average-sized asperities, this is insufficient for the outlying features to which these parameters correspond. As such, the tallest asperities were still forced into direct contact and aggressively reduced in height.

For Rv, U appeared to protect the fast surface but induced a greater reduction in the slow surface value. The change in Rv parameter, whilst representing the depth to the deepest valley points, can perhaps be better thought of as a measure of the change in the height of the mean line through running-in. As features above the mean line are removed from the profile, the mean line moves down relative to the profile, reducing the depth of the deepest valleys when measured from the mean line. Closer examination of the slow surface results for Rv showed significant influence from a single outlying result from Test 2, in which wear was induced. While it was attempted to remove wear-affected profiles from the analysis, it is possible that this wear induced a more aggressive removal of protruding features, and consequently a greater decrease in the mean line height, thus causing the observed U effect. The reduced influence of

U on the slow surface Rz is also likely to be influenced by that outlying result.

The SRR did not show consistent effects between the fast and slow surfaces. Typically, the fast surface results showed that increased SRR led to a greater magnitude of change in the considered parameters, flattening and reducing the height of roughness features similarly to the effect of P. On the slow surface however SRR commonly showed minimal influence on the outcome. For the “element-wise parameters,” Rc, mean asperity height, and mean asperity CSA, the direction of the slow surface effect was inconsistent. For these parameters, the results at high and low SRR showed a large amount of overlap, making it likely that further repeats of the test program would show SRR to actually have negligible influence on these parameters.

Mean radius of curvature of asperities was strongly affected by SRR for both surfaces, likely due to increased abrasive action and heat generation resulting from the increase in sliding.

Sliding is known to increase the loading cycles on asperities, and expose them to a greater number of different

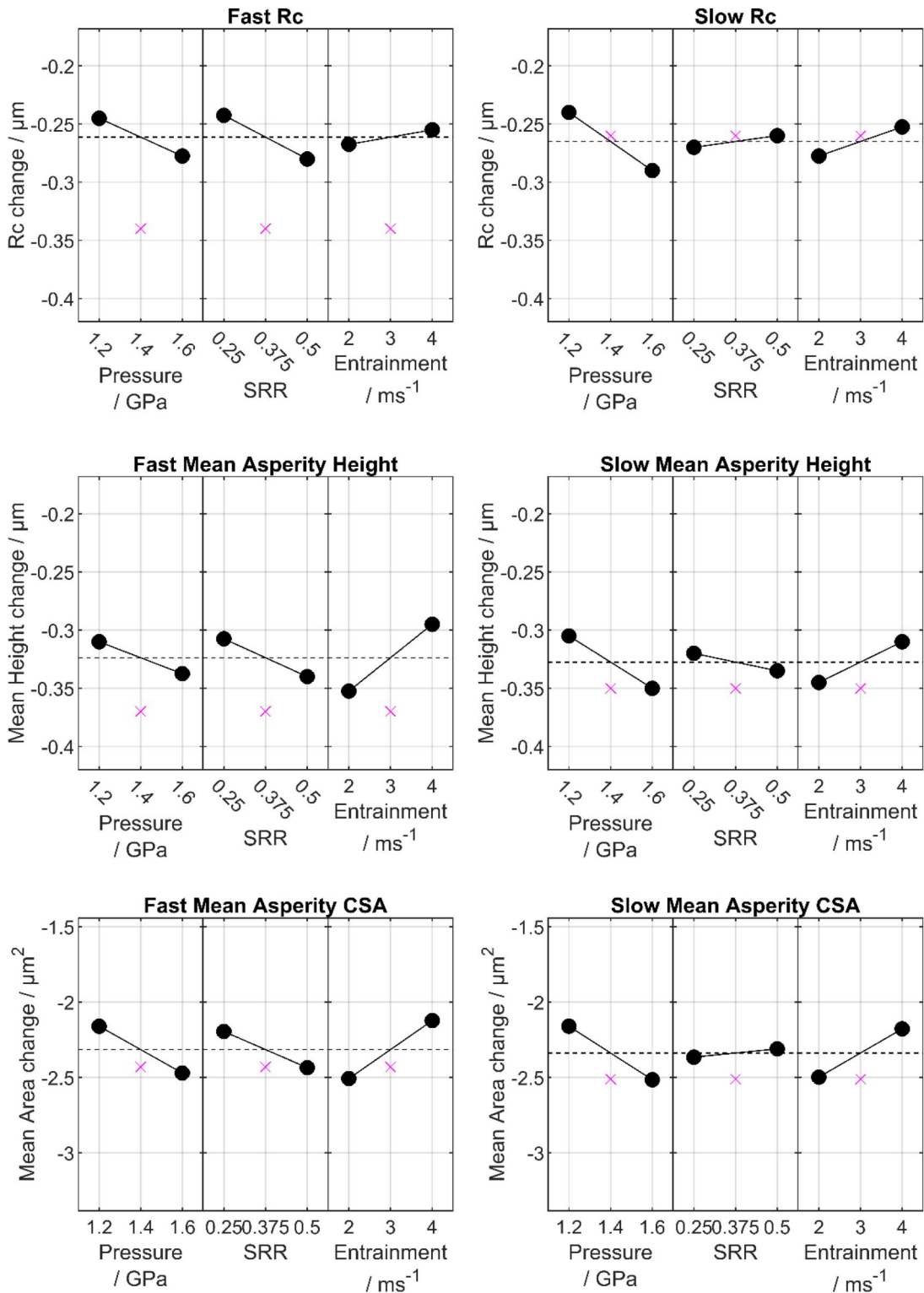


**Figure 17.** Main effects of pressure (P), slide-roll ratio (SRR), and entrainment (U) on Rc, mean asperity height, and mean asperity cross-sectional area (CSA) for the fast and slow surfaces. Note the finer vertical axis scale for Rv.

roughness features on the opposing surface as sliding increases. This has been argued as an effect on fatigue, with some potential dependence on the direction of sliding due to surface cracks, (28–30) however, has not been widely explored in terms of running-in. The cause of the changing influence of sliding on running-in depending on whether it is the fast or slow surface in consideration therefore remains unresolved.

The results of this experimental investigation showed the running-in process to be influenced by a large number of both two- and three-factor interaction effects. These effects varied by parameter, but some parameters did share common interaction effects. One such example is that the protective influence of U was often more effective when P was low than when P was high (Ra, Rq, Rp, Rz, Rc, mean

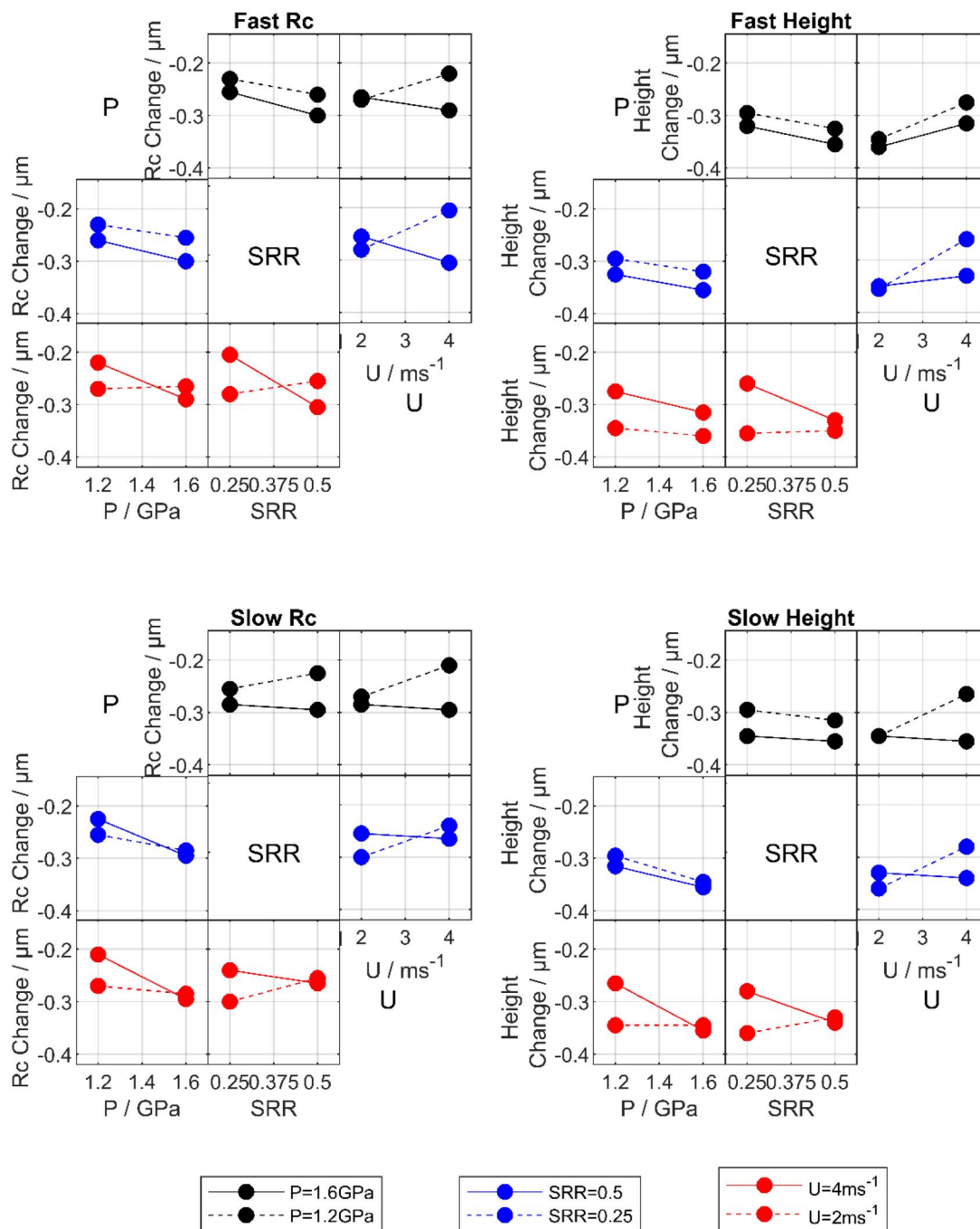


**Figure 18.** Two-factor interaction plots between pressure (P), slide-roll ratio (SRR), and entrainment (U) for Rc and mean asperity height on the fast and slow surfaces.

asperity height). That these interactions were present in the results, and also that even more complex three-factor interactions were observed, provides evidence that running-in is a complex process with interconnected inputs. These processes may influence the surfaces through a variety of mechanisms such as thermal effects, frictional effect, or metallurgical transformations, and merit further in-depth investigation. The ability to clearly discern these multifactor interaction effects without confounding (where the influences of groups of individual- and multi-factor effects become inextricable) is due to the novel application of a full-factorial experimental design applied in this work. Previous works have applied fractional factorial designs to investigate micro-pitting fatigue to excellent effect (25,30,31) but were

inherently unable to separate some factors and multi-factor effects, leading to the necessary assumption that some multi-factor effects have zero effect. This paper has further built upon that work, extended the investigation to the effects on running-in, and has subsequently shown that it is necessary to consider that P, SRR, and U have non-zero interaction effects, which have an appreciable impact on surface modification during running in.

It is noted that initial roughness is known to have an influence on running-in and subsequent fatigue. In this experimental program initial roughness ( $R_a$ ) was controlled to within a window of approximately  $\pm 0.05 \mu\text{m}$  through the manual and somewhat iterative disk grinding process, leaving some variation much like that encountered in

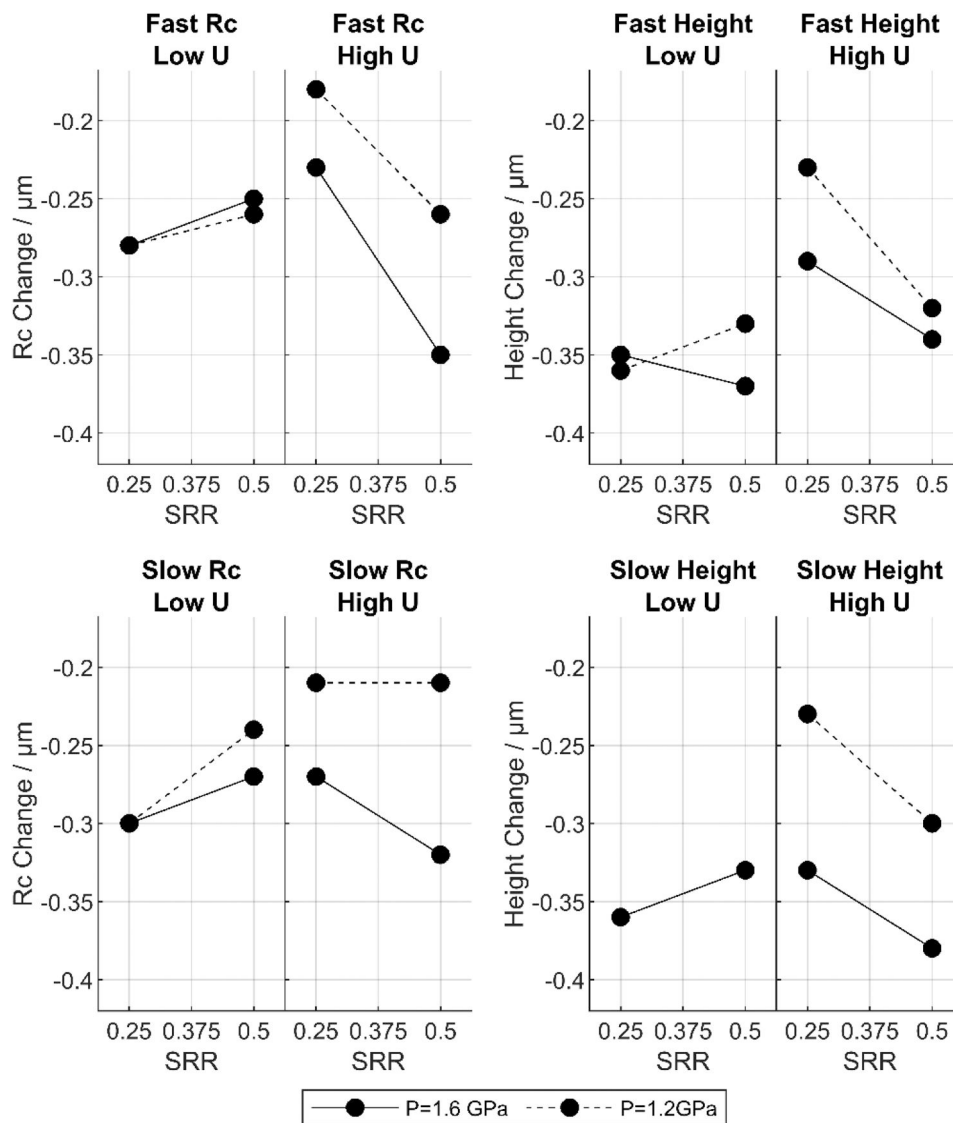


Figure 19. The pressure (P) and slide-roll ratio (SRR) interactions at low and high entrainment (U) for Rc and mean asperity height on the fast and slow surfaces.

commercial gears. Disks were allotted to tests at random to reduce potential effects of roughness variation; however, due to the duration of each test—each requiring approximately 1 month to prepare and run—it was not possible to run repeat tests without rendering the test program unmanageable. It is therefore noted that the accuracy of the effects of each individual and multi-factor effect may improve with future work.

## Conclusions

- A full-factorial experimental program was conducted to assess the influence of P, SRR, and U on ground surfaces through running-in. This provides a novel assessment of the effects of both individual- and multivariable effects, free from confounding.
- The P increased the change in the surface through running-in, reducing surface roughness and height parameters, and increasing the radius of curvature of asperities.

- Increased U protected the surface through generation of a thicker lubricant film. This protection did not extend to the largest asperity peaks ( $R_p$ ,  $R_z$ ) which still exceeded the film and were reduced in height.
- SRR behaved differently on fast and slow surfaces. While SRR increased change in the fast surface, it typically had minimal influence on the slow surface.
- Two- and three-factor interactions were seen for all parameters, showing running-in to be a result of complex individual and interaction effects.

## Disclosure statement

The authors report that there are no competing interests to declare.

## Data access statement

Information on the data underpinning both Parts 1 and 2 of this publication, including access details, can be found in the Cardiff University Research Data Repository at <http://doi.org/10.17035/cardiff.26997361>.

**Table 4.** Effect strengths for each factor and interaction on the fast and slow surfaces.

Parameter	Fast Surface						
	P	SRR	U	P*SRR	P*U	SRR*U	P*SRR*U
Mean Cross-Sectional Area / $\mu\text{m}^2$	-0.31 (-0.81)	-0.24 (-0.62)	0.385 (1.00)	-0.08 (-0.21)	-0.025 (-0.06)	-0.265 (-0.69)	-0.285 (-0.74)
Mean Asperity Height / $\mu\text{m}$	-0.028 (-0.48)	-0.033 (-0.57)	0.058 (1.00)	-0.003 (-0.05)	-0.013 (-0.22)	-0.038 (-0.66)	-0.023 (-0.40)
Ra / $\mu\text{m}$	-0.015 (-0.83)	-0.005 (-0.28)	0.01 (0.56)	0 (0.00)	-0.015 (-0.83)	-0.015 (-0.83)	0 (0.00)
Rc / $\mu\text{m}$	-0.033 (-0.52)	-0.038 (-0.60)	0.013 (0.21)	-0.008 (-0.13)	-0.038 (-0.60)	-0.063 (-1.00)	0.013 (0.21)
RoC / $\mu\text{m}$	18.798 (0.76)	24.573 (1.00)	-16.163 (-0.66)	8.048 (0.33)	-13.688 (-0.56)	-3.593 (-0.15)	11.678 (0.48)
Rp / $\mu\text{m}$	-0.033 (-0.18)	-0.053 (-0.28)	0.018 (0.10)	0.063 (0.34)	-0.077 (-0.41)	-0.188 (-1.00)	0.013 (0.07)
Rq / $\mu\text{m}$	-0.015 (-0.54)	-0.02 (-0.71)	0.01 (0.36)	0 (0.00)	-0.01 (-0.36)	-0.015 (-0.54)	-0.005 (-0.18)
Rt / $\mu\text{m}$	-0.51 (-0.77)	-0.275 (-0.42)	-0.315 (-0.48)	-0.225 (-0.34)	-0.555 (-0.84)	-0.66 (-1.00)	0.45 (0.68)
Rv / $\mu\text{m}$	-0.06 (-0.92)	-0.04 (-0.62)	0.025 (0.38)	-0.025 (-0.38)	0 (0.00)	-0.02 (-0.31)	0.015 (0.23)
Rz / $\mu\text{m}$	-0.093 (-0.44)	-0.088 (-0.41)	0.043 (0.20)	0.043 (0.20)	-0.078 (-0.37)	-0.213 (-1.00)	0.033 (0.15)
Parameter	Slow Surface						
	P	SRR	U	P*SRR	P*U	SRR*U	P*SRR*U
Mean Cross-Sectional Area / $\mu\text{m}^2$	-0.355 (-0.92)	0.055 (0.14)	0.32 (0.83)	-0.105 (-0.27)	-0.24 (-0.62)	-0.1 (-0.26)	-0.22 (-0.57)
Mean Asperity Height / $\mu\text{m}$	-0.045 (-0.78)	-0.015 (-0.26)	0.035 (0.60)	0.005 (0.09)	-0.045 (-0.78)	-0.045 (-0.78)	-0.005 (-0.09)
Ra / $\mu\text{m}$	-0.018 (-1.00)	-0.002 (-0.11)	0.007 (0.39)	-0.007 (-0.39)	-0.018 (-1.00)	-0.013 (-0.72)	0.007 (0.39)
Rc / $\mu\text{m}$	-0.05 (-0.79)	0.01 (0.16)	0.025 (0.40)	-0.02 (-0.32)	-0.035 (-0.56)	-0.035 (-0.56)	0.005 (0.08)
RoC / $\mu\text{m}$	14.828 (0.60)	15.813 (0.64)	-10.103 (-0.41)	13.418 (0.55)	-1.647 (-0.07)	-5.833 (-0.24)	-3.983 (-0.16)
Rp / $\mu\text{m}$	-0.087 (-0.46)	0.013 (0.07)	0.018 (0.10)	-0.108 (-0.57)	-0.133 (-0.71)	-0.123 (-0.65)	0.073 (0.39)
Rq / $\mu\text{m}$	-0.028 (-1.00)	-0.002 (-0.07)	0.007 (0.25)	-0.007 (-0.25)	-0.018 (-0.64)	-0.013 (-0.46)	0.007 (0.25)
Rt / $\mu\text{m}$	-0.463 (-0.70)	0.033 (0.05)	0.158 (0.24)	-0.383 (-0.58)	-0.258 (-0.39)	-0.123 (-0.19)	-0.053 (-0.08)
Rv / $\mu\text{m}$	-0.03 (-0.46)	-0.01 (-0.15)	-0.02 (-0.31)	-0.015 (-0.23)	-0.015 (-0.23)	-0.065 (-1.00)	0.03 (0.46)
Rz / $\mu\text{m}$	-0.12 (-0.56)	0.01 (0.05)	-0.01 (-0.05)	-0.125 (-0.59)	-0.145 (-0.68)	-0.185 (-0.87)	0.1 (0.47)

Abbreviations: P, pressure; SRR, slide-roll ratio; U, entrainment.

## Funding

The authors would like to acknowledge the support of EPSRC, who funded the studentship that carried out much of this work via the Doctoral Training Partnership, and BMT Limited, for their generous support of the first author's involvement in the production of this paper.

## References

- (1) Krantz, T. L., Alanou, M. P., Evans, H. P., and Snidle, R. W. (2001), "Surface Fatigue Lives of Case-Carburized Gears with an Improved Surface Finish," *Journal of Tribology*, **123**, pp 709–716. doi:10.1115/1.1387036
- (2) Tallian, T. E. (1967), "On Competing Failure Modes in Rolling Contact," *A S L E Transactions*, **10**, pp 418–439. doi:10.1080/05698196708972201
- (3) Spikes, H. and Guangteng, G. (1997), "An Experimental Study of Film Thickness in the Mixed Lubrication Regime," *Elastohydrodynamics '96: Fundamentals and Applications in Lubrication and Traction*, ed. D. Dowson, C. M. Taylor, T. H. C. Childs, G. Dalmaz, Y. Berthier, L. Flamand, J.-M. Georges, and A. A. Lubrecht, pp 159–166, Elsevier: Amsterdam.
- (4) Sharif, K. J., Evans, H. P., and Snidle, R. W. (2012), "Modelling of Elastohydrodynamic Lubrication and Fatigue of Rough Surfaces: The Effect of Lambda Ratio," *Proceedings of the Institution of Mechanical Engineers, Part J: J Engineering Tribology*, **226**, pp 1039–1050. doi:10.1177/1350650112458220
- (5) Clarke, A., Weeks, I. J. J., Snidle, R. W., and Evans, H. P. (2016), "Running-In and Micropitting Behaviour of Steel Surfaces under Mixed Lubrication Conditions," *Tribology International*, **101**, pp 59–68. doi:10.1016/j.triboint.2016.03.007
- (6) Sosa, M., Björklund, S., Sellgren, U., and Olofsson, U. (2015), "In Situ Surface Characterization of Running-In of Involute Gears," *Wear*, **340-341**, pp 41–46. doi:10.1016/j.wear.2015.03.008
- (7) Hansen, J., Björling, M., and Larsson, R. (2020), "Topography Transformations Due to Running-In of Rolling-Sliding Non-Conformal Contacts," *Tribology International*, **144**, 106126. doi:10.1016/j.triboint.2019.106126
- (8) Bishop, I. F. and Snidle, R. W. (1984), *An Investigation of Alternative Methods of Quantifying Running-In of Surfaces*, Society of Automotive Engineers: Warrendale, PA.
- (9) Kelly, D. A., Barnes, C. G., and Rudd, L. M. (1998), "Aspects of Thrust Cone Tribology: Part 1: Effects of Slide to Roll Ratio on Surface Failure Mechanisms in Twin-Disc Tests," *Proceedings of the Institution of Mechanical Engineers, Part J: Journal of*

- Engineering Tribology*, **212**, pp 55–72. doi:10.1243/1350650981541895
- (10) Lohner, T., Mayer, J., Michaelis, K., Höhn, B.-R., and Stahl, K. (2017), “On the Running-In Behavior of Lubricated Line Contacts,” *Proceedings of the Institution of Mechanical Engineers, Part J: Journal of Engineering Tribology*, **231**, pp 441–452. doi:10.1177/1350650115574869
- (11) Wang, W., Wong, P. L., and Zhang, Z. (2000), “Experimental Study of the Real Time Change in Surface Roughness during Running-In for PEHL Contacts,” *Wear*, **244**, pp 140–146. doi:10.1016/S0043-1648(00)00448-8
- (12) Sjöberg, S., Sosa, M., Andersson, M., and Olofsson, U. (2016), “Analysis of Efficiency of Spur Ground Gears and the Influence of Running-In,” *Tribology International*, **93**, pp 172–181. doi:10.1016/j.triboint.2015.08.045
- (13) Prajapati, D. K. and Tiwari, M. (2019), “Assessment of Topography Parameters During Running-In and Subsequent Rolling Contact Fatigue Tests,” *Journal of Tribology*, **141**, 051401. doi:10.1115/1.4042676
- (14) Cabanettes, F. and Rosén, B.-G. (2014), “Topography Changes Observation during Running-In of Rolling Contacts,” *Wear*, **315**, pp 78–86. doi:10.1016/j.wear.2014.04.009
- (15) Martins, R., Locatelli, C., and Seabra, J. (2011), “Evolution of Tooth Flank Roughness during Gear Micropitting Tests,” *Industrial Lubrication and Tribology*, **63**, pp 34–45. doi:10.1108/00368791111101821
- (16) Hutt, S., Clarke, A., and Evans, H. P. (2018), “Generation of Acoustic Emission from the Running-In and Subsequent Micropitting of a Mixed-Elastohydrodynamic Contact,” *Tribology International*, **119**, pp 270–280. doi:10.1016/j.triboint.2017.11.011
- (17) Sosa, M., Sellgren, U., Björklund, S., and Olofsson, U. (2016), “In Situ Running-In Analysis of Ground Gears,” *Wear*, **352–353**, pp 122–129. doi:10.1016/j.wear.2016.01.021
- (18) Blau, P. J. (2005), “On the Nature of Running-In,” *Tribology International*, **38**, pp 1007–1012. doi:10.1016/j.triboint.2005.07.020
- (19) Lugt, P. M., Severt, R. W. M., Fogelström, J., and Tripp, J. H. (2001), “Influence of Surface Topography on Friction, Film Breakdown and Running-In in the Mixed Lubrication Regime,” *Proceedings of the Institution of Mechanical Engineers, Part J: Journal of Engineering Tribology*, **215**, pp 519–533. doi:10.1243/1350650011543772
- (20) Clarke, A., Weeks, I. J. J., Evans, H. P., and Snidle, R. W. (2016), “An Investigation into Mixed Lubrication Conditions Using Electrical Contact Resistance Techniques,” *Tribology International*, **93**, pp 709–716. doi:10.1016/j.triboint.2014.10.010
- (21) Defence Procurement Agency, Defence Standard 91-74, Lubricating Oil, Team Turbine and Gear, Extreme Pressure Joint Service Designation OEP-80 (n.d).
- (22) NIST/SEMATECH (2013), NIST-SEMATECH e-Handbook of Statistical Methods, NIST, <https://www.itl.nist.gov/div898/handbook/index.htm> (accessed January 6, 2021).
- (23) Crump, M. J. C., Navarro, D., and Suzuki, J. (2019), “Answering Questions with Data: Introductory Statistics for Psychology Students,” [10.17605/OSF.IO/JZE52](https://doi.org/10.17605/OSF.IO/JZE52) (accessed January 6, 2021).
- (24) Roberts, D. P. (2017), *Analysis of Gear Running-In Experimental Data*. Cardiff University: Cardiff, UK.
- (25) Li, S. and Kahraman, A. (2013), “Micro-Pitting Fatigue Lives of Lubricated Point Contacts: Experiments and Model Validation,” *International Journal of Fatigue*, **48**, pp 9–18. doi:10.1016/j.ijfatigue.2012.12.003
- (26) Mallipeddi, D., Norell, M., Sosa, M., and Nyborg, L. (2017), “Influence of Running-In on Surface Characteristics of Efficiency Tested Ground Gears,” *Tribology International*, **115**, pp 45–58. doi:10.1016/j.triboint.2017.05.018
- (27) Olver, A. (2002), “Gear Lubrication – A Review,” *Proceedings of the Institution of Mechanical Engineers, Part J: Journal of Engineering Tribology*, **216**(5), pp 255–267. doi:10.1243/135065002760364804
- (28) Olver, A. V., Tiew, L. K., Medina, S., and Choo, J. W. (2004), “Direct Observations of a Micro-pit in an Elastohydrodynamic Contact,” *Wear*, **256**, pp 168–175. doi:10.1016/S0043-1648(03)00374-0
- (29) Qiao, H., Evans, H. P., and Snidle, R. W. (2008), “Comparison of Fatigue Model Results for Rough Surface Elastohydrodynamic Lubrication,” *Proc IMechE Vol. 222 Part J: J Engineering Tribology Proceedings of the Institution of Mechanical Engineers, Part J: Journal of Engineering Tribology*, **222**, pp 381–393. doi:10.1243/13506501JET347
- (30) Morales-Espejel, G. E., Rycerz, P., and Kadircic, A. (2018), “Prediction of Micropitting Damage in Gear Teeth Contacts Considering the Concurrent Effects of Surface Fatigue and mild wear,” *Wear*, **398–399**, pp 99–115. doi:10.1016/j.wear.2017.11.016
- (31) Oila, A., and Bull, S. J. (2005), “Assessment of the Factors Influencing Micropitting in Rolling/Sliding Contacts,” *Wear*, **258**, pp 1510–1524. doi:10.1016/j.wear.2004.10.012

## Appendix

Figure A1 shows a typical result from the first running-in stage (3,000 fast disk cycles) of Test 4, in order to illustrate the typical contact voltage, friction and temperature behavior seen during the running-in tests.

During the test, the disk temperature initially rises due to frictional heating, before near-equilibrium conditions are reached during the second half of the test stage. The friction signal falls slightly over the test stage, from around 100 N at the start, to around 95 N at the conclusion of the test stage. This decrease is due to the reduction in height of the most aggressive asperities leading to a consequent decrease in the level of asperity interaction and metallic friction.

This behavior is confirmed by the contact voltage measurements. These measurements indicate the amount of asperity interaction occurring. For the contact voltage setup used on this test rig, the signal can range between a maximum of 43 mV (indicative of full film conditions with no direct asperity contact occurring) and a minimum of 0 mV when there are high levels of asperity contact. Previous work (20) has shown the system to be sensitive to contact conditions for values of  $\Lambda$  below 2, and to be highly sensitive below  $\Lambda = 1.2$  with an almost linear relationship between  $\Lambda$  and contact voltage in this region. For this example of Test 4, the contact voltage has an initial value of around 8 mV. By the end of the running-in stage, at 3,000 fast disk cycles, the contact voltage has increased to around 17 mV. This indicates that the amount of asperity interaction has reduced as a consequence of the surface topography changes occurring during running-in. These results are consistent with the results shown in (20) and are typical of those seen during these experiments.

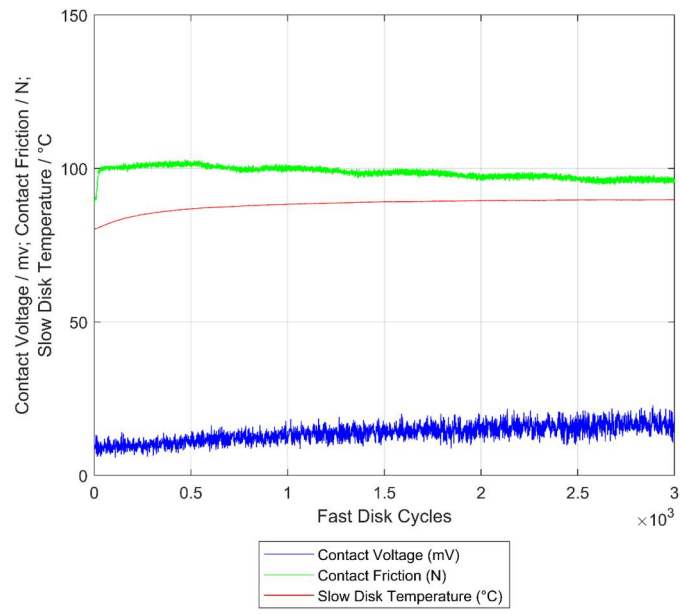


Figure A1. Variation of contact voltage, friction and disk temperature during the first running-in stage of Test 4.